Determination of the Magnetic Background Field on Naval Ships

A.C. Lumadjeng

A thesis submitted in partial fulfillment for the degree
BACHELOR IN SCIENCE

in

INDUSTRIAL AND APPLIED MATHEMATICS
University of Technology Delft

Supervisors: Ir. A.R.P.J. Vijn, Dr.Ir. E.S.A.M. Lepelaars

August 2017

Abstract

For my bachelor's graduation project, I did an internship at TNO, working on a project for the Ministry of Defence. This thesis describes and discusses the project that looked for a prediction model for the magnetic background field on a naval ship. The prediction model that was developed during this project separates the magnetic background field from other existing, observed magnetic fields. Determination of the magnetic background field on naval ships helps the reduction of detection risk. Further research and fine tuning of this model might be of use to The Royal Dutch Navy in order to avoid any risk of detonation of naval mines in threat areas.

Acknowledgements

I would like to thank Aad Vijn (TUD) and Eugène Leplaars (TNO) for their pleasant support throughout my graduation project and internship at TNO. They have always been very patient with me and always made me want to learn more. They reviewed many drafts of this thesis, giving me the opportunity to learn from my mistakes and to grow as the project went on. Also, I thank Eugène for making the Seven Sensors array, so that I could use it to perform measurements.

Lastly, I thank my fellow interns and colleagues at TNO for all their support. They always made me take a quick break, even if I thought I didn't need it. I would like to thank them for all the pleasant conversations and the offers for reviewing my thesis.

Contents

Chapter 1

Introduction

1.1 Motivation

We could say that the earth is one big magnet. Earth's core is fluid iron, which means that the iron can move around. This induces a magnetic field around the earth, not only making the earth itself a magnet, but making every object on earth of metal material, magnetic too. We call this field the (earth's) magnetic background field. This project specifically looked at the magnetic background field of a naval vessel and explains how it is determined

Because naval vessels are made of steel, which is a ferromagnetic material, they disturb the earth's magnetic field locally. This disturbance is called the *magnetic signature* of a naval vessel, and can be detected by modern naval mines, by means of a magnetic sensor. The notion of magnetic signature will be further explained in section 1.1.1. After detection, localization and classification of a naval vessel by a naval mine, the mine can decide to actuate. As the Royal Dutch Navy often operates in areas where naval mines are present, the risk of any detonation must be avoided, for higher chance of mission success. The motivation for this research is the threat naval vessels face at sea in areas where the threat of naval mines is high.

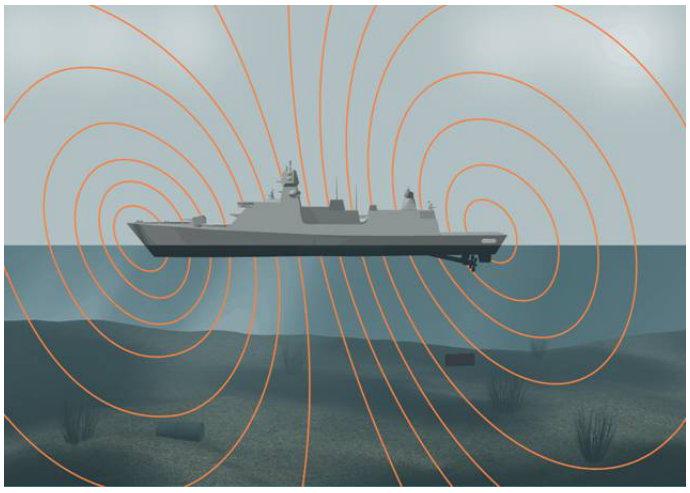

Figure 1.1: The magnetic signature of a naval vessel, which can be detected by a mine resting on the bottom of the ocean [1].

Today, the Netherlands Organization for Applied Scientific Research (TNO), is working together with the Delft University of Technology (TUD) for the Dutch Ministry of Defence to reduce the threat against naval vessels and improving its safety. They are developing advanced numerical models for the next generation of marine ships to further reduce the risk of detection by naval mines.

1.1.1 The magnetic signature of a naval vessel

The *signature* of a naval ship is the complete collection of influences a naval ship has on its environment, see Figure 1.2. Because a naval mine is able to detect the signature of a naval ship, our goal is to manipulate and minimize the influences of the vessel. This project only contemplates the magnetic influences, or *magnetic signature* of a naval ship. To reduce the risk of magnetic visibility to a naval mine that is able to observe the magnetic signature, we have to know accurately what the value of the magnetic signature is.

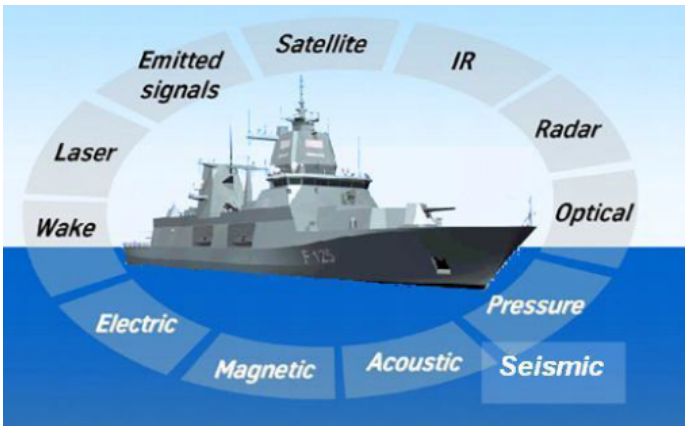

Figure 1.2: The collection influences of a naval ship [3].

So far, two different types of magnetic fields have been mentioned. The magnetic background field and a magnetic field of a naval ship. We define these two as followed as the difference should be clear.

- **Magnetic background field**. This is a field induced by earth's fluid iron core, earlier called earth's magnetic field. So essentially, this field is always present. The magnetic background field is also considered to be locally uniform because the direction of the magnetic background field changes very little over long distances.
- **Magnetic distortion field**. When a steel object (i.e., a ship) is placed anywhere on earth, the magnetic background field is disturbed by another field, induced by the presence of the steel object. This other field is defined as the magnetic distortion field.

Now that we know the difference between these two fields, we can define what the magnetic signature is. The magnetic signature of a naval ship is defined as the magnetic distortion field that consists all other distortion fields caused by the steel objects in or on the naval vessel, and the vessel itself. The sum of the magnetic background field and the magnetic distortion field are defined as the *total magnetic field* around a naval vessel.

Imagine no ship is present, then the magnetic background field remains undisturbed. The Figures 1.3a and 1.3b show what happens to the background field when a ship passes by. Thus the new field, illustrated in Figure 1.3b is the total magnetic field consisting of the magnetic background field, illustrated in Figure 1.3a, and the magnetic distortion field caused by the ship. Now, we are interested in this disturbed field, because a naval mine detects the difference between Figures 1.3a and 1.3b, that influence of the magnetic signature.

1.1.2 The naval mine

The first naval mine was deployed against the British fleet by the colonialist during the American Revolutionary War. This mine was actually a floating tar covered beer keg filled with gunpowder. These

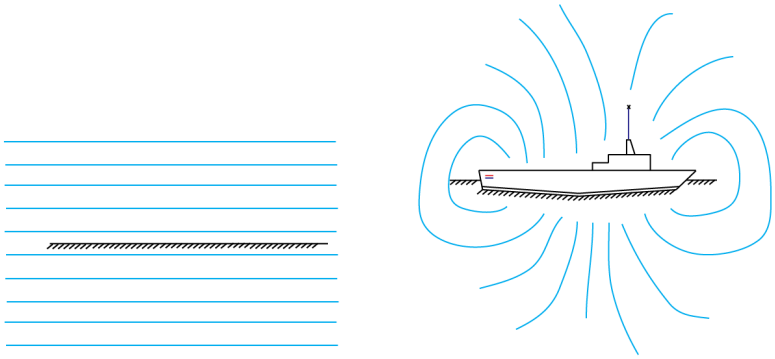

(a) A uniform, undisturbed field at sea.

(b) The disturbed field, caused by a steel object.

Figure 1.3: The influence of a naval ship on the magnetic background field.

old mines would actually only detonate when they came in contact with the target [6]. These mines were eventually found to be unreliable due to their touchy firing mechanism and wet gunpowder. Further development of contact mines resulted in many different mines, some working and some ineffective.

The modern influence mine

One of the mines that is considered effective, is the modern influence mine, resting on the bottom of the ocean in shallow waters. This means we can not simply sail around it, because we can not see where it is. It uses modern magnetic mine technologies to detect the influences of near ships. By influences, we mean the signals as shown in Figure 1.2. Examples of signals a naval vessel unintentionally generates include magnetic fields, electric fields, acoustic waves and pressure waves. These signals are detectable by all kinds of sensors on the influence mine and a clever algorithm will determine if a ship is nearby (localization), after which it can decide to actuate. The exact activity within a naval mine is currently classified, and so it is not clear what a naval mine further classifies before detonating.

Figure 1.4: The Italian MN103 Manta mine, resting on the bottom of shallow waters [2].

1.2 Defence's ultimate goal

To avoid detonation of naval mines, we need to reduce the magnetic signature. In order to do that, we require an accurate description of the magnetic signature. Right now, we are not able to come up with that description as there are some complications. We are able to measure the magnetic field at a certain location, using a magnetic sensor, but the complication lies in the fact that the magnetic

field we measure with a sensor is the total magnetic field and not just the magnetic signature. By the principle of superposition, we know that this total field consists of the magnetic signature and the magnetic background field. Thus at sea, we are not able to measure just the magnetic signature of a ship directly. Because a ship is made completely out of steel, we will always measure the disturbed, total magnetic field because of its magnetizing ability.

Now the ultimate goal to reach safety, is to reduce the magnetic signature to such an extent that naval mines no longer measure the change the steel vessel causes. However, because we measure the total magnetic field, instead of just the magnetic signature, the goals are as followed:

- **Monitoring magnetic signature**. If we are able to detect and visualize the magnetic signature, we are able to start reducing the threat to naval vessels.
- **Reduce the magnetic signature of a naval vessel**. When there has been found a way to monitor solely the magnetic signature of a naval vessel, the ultimate goal is to reduce the magnetic signature.

These goals go beyond this project and the research goals for this project will be defined later on in chapter two. Evidently, the goals for this project align with the interests of the ultimate goal.

1.2.1 Existing methods to reducing the threat

It may seem like detecting the magnetic signature of a naval vessel to avoiding threat is completely impossible. Naturally, that is not true as there are some methods today that reduce threat against naval ships caused by naval mines. The last naval vessel of The Royal Netherlands Navy that was hit by a naval mine was possibly in the Second World War [6].

Minehunters and minesweepers

A minehunter is a naval vessel that actively seeks, detects and destroys naval mines. It uses sonar images to detect the targets and sends out an nonmagnetic minehunting explosive [7]. There are also minesweepers, who differ in prior detection of targets. A minesweeper is a small amagnetic naval warship that just cleans up all the mines in the water by diffusing the detonation-mechanism [7].

(a) The USS Raven MHC 61, an American minehunter

(b) A minehunting ROV of the German Navy

(c) The Dutch Hr.Ms.Mercuur, an old minesweeper

Figure 1.5: Examples of nonmagnetic vessels [7].

A degaussing system

Today, a naval vessel is able to degauss a magnetic field. *Degaussing* is the process of decreasing or eliminating a magnetic field. This process is named after the gauss, a unit of magnetism. Degaussing is done by a degaussing system which is a system that consists of several electromagnetic coils, spread throughout the ship. Each coil is placed in either the x, y or z-direction. A degaussing system can be

found in the hull of a naval vessel. In order for a degaussing system to optimally reduce the magnetic signature, the magnetic background field is needed. This is obtained by placing a sensor in the mast.

A sensor in the mast

Not being able to measure the magnetic signature separately on board, does not mean measuring on board is totally useless. This method places a sensor in its mast and measures the magnetic field around it. Because of the lack of any algorithm or dipole model, naval ships assume this field to be the undisturbed magnetic background field and uses this field to monitor the magnetic signature and to reduce it, using the degaussing system.

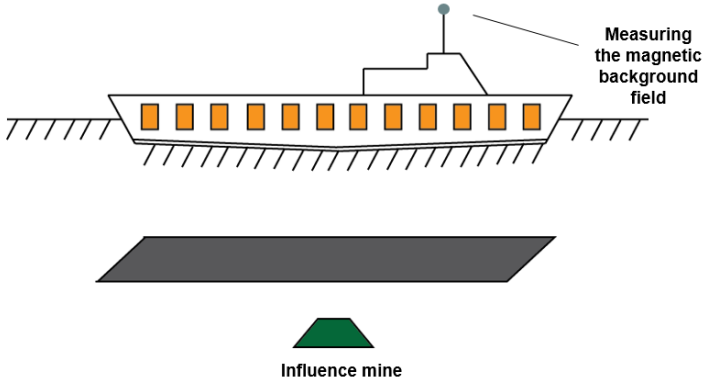

Figure 1.6: Measuring the magnetic background field with a sensor in the mast.

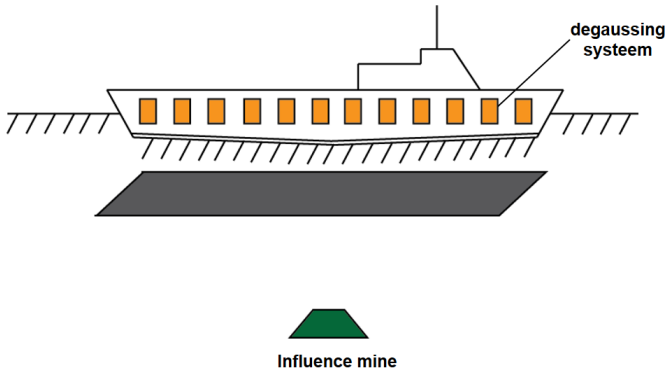

Figure 1.7: The works of a degaussing system to reduce the magnetic signature.

The plane below the ship represents a certain location where the naval mine is still able to detect the vessel's magnetic signature. Reducing the magnetic signature would mean the imaginary plane rises closer to the ship. The goal is to do this to such an extent that the distance between the plane and the naval mine is sufficiently large such that the magnetic signature is not detected by the mine anymore.

The Royal Dutch Navy uses the sensor in the mast together with a degaussing system on board. The sensor in the mast measures the magnetic field and as mentioned earlier, it is assumed that this collection of fields is the magnetic background field. Then an algorithm, depending on a measured magnetic background field, controls the flow of electricity to the degaussing system, manipulating the magnetic signature. The magnetic background field of the earth can not be manipulated, but a successful

algorithm will reduce the magnetic signature. However, for practical reasons, it is not possible to reduce a magnetic field completely to zero.

An important note of this method is that one sensor only gives one data point that actually measures a collection of fields, but assumes this measurement to represent the undisturbed, magnetic background field. Therefore, we are again questioning the reliability of this method. In reality, this method works quite well and is actively in use, but this research serves to find another method where this assumption is not made.

1.3 The goal of this research

We have come to aim of my project. To formulate the research goals properly, we take a look at the problem up until this point.

The problem

To reduce the risk of detection by naval mines, we want to reduce the magnetic signature of a naval ship. The magnetic field around a naval vessel is acquired by measuring on board, however when this is done, we measure the total magnetic field, when we actually just want the magnetic distortion field (magnetic signature). Knowing that the total magnetic field is the sum of the magnetic distortion field and the magnetic back ground field, we can determine the magnetic signature if the magnetic background field is known to us.

The goal

The aim of this research is to develop a prediction model, to determine the background field, based on magnetic measurements in the vicinity of a magnetic disturber such as a ship. Furthermore, we try to improve the method used today, which measures with one sensor in the mast and assuming the measured field to be the magnetic background field. We investigate if there is any added value in a new method using a sensor array, instead of the single sensor, to obtain a more accurate estimate of the background field.

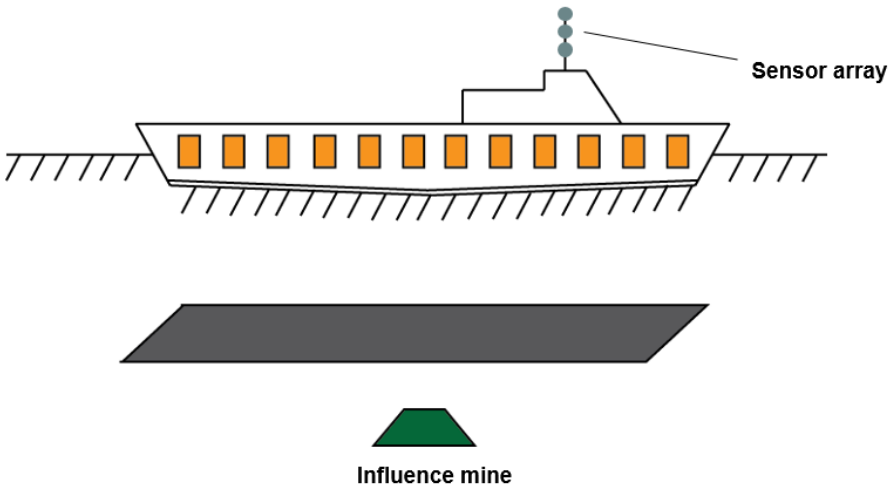

Figure 1.8: The idea of the use of a sensor array to obtain a more accurate magnetic background field.

The summary of these goals allows to define two main goals of this project:

- **Determination of the magnetic background field**. The first main goal is to determine an accurate approximation of the magnetic background field using a dipole model and sensor array for measurements.
- **Improve the current method**. The second main goal is to improve the method that is used today, obtaining data by a single sensor.

1.3.1 The process to achieving the goal

This prediction model is tested on a setup, smaller, but resembling the situation of a naval vessel at sea. We constructed a small mast consisting of seven sensors. We use this device, the Seven Sensors, to create two situations:

- The Seven Sensors can be used as a sensor array used to obtain several data points, to determine an accurate magnetic background field.
- Considering only one sensor of the Seven Sensors-array, the method we have today is recreated. We can measure the magnetic field using one sensor, and assume this to be the magnetic background field.

In this thesis, we consider the following topics essential to the main goal of this project:

- **Determination of a correct formulation of the prediction model**. The model we use to determine the magnetic background field formulates a so-called forward problem and solves an inverse problem, which will be fully explained and demonstrated in later chapters.
- **Accuracy of the prediction model using the sensor array**. If the obtained magnetic background field is found to be accurate, we are one step closer to finding out if this new method has any added value to the method the navy uses today.
- **Reproducing the existing method using one sensor**. In order to improve the method used today, we should have some comparison material. Therefore, we compute the magnetic background field using one sensor, recreating the method the Royal Dutch Navy uses today.
- **The value of the prediction model using the sensor array.** Lastly, we perform simulations and conduct an experiment to see if the model developed during this project is able to compute a more accurate magnetic background field than if we were to use the existing method.

In this report the above research topics are considered and answered.

1.4 Chapter outline

To get a clear image of what this thesis will contain, the content of the chapters are outlined as followed. In chapter two, we derive an analytical; expression for the magnetic induction field $\mathbf{B}$, which can be used to compute any magnetic field $\mathbf{H}$. In chapter three, the prediction model is explained and we see that it relies on a forward problem and an inverse problem which will both be explained and formulated in the following two chapters. Chapter five also discusses a criterion, based on approximation errors, that determines if the prediction model accurate. As there is always some noise in real data, we also considered white Gaussian noise for this project. Chapter six describes the noise model and where numerical instability in solving the model might come from. In particular, we look at the use of singular value decomposition for the model which causes some unrealistic results. Chapter seven discusses regularization methods and the revised model, using a regularization method is tested in a simulation in chapter eight. Finally, chapter 9 will perform the experiment on the Seven Sensors and we see if the developed prediction model works. Chapter 10 discusses and analyzes the results after which we have arrived at a conclusion.

Chapter 2

The magnetic field of a magnetic point dipole

In chapter 1, several kinds of magnetic fields are mentioned. This chapter defines these fields as mathematical objects and constructs an expression for the magnetic field of a magnetic point dipole. We can consider a magnetic point dipole to be a small magnetic object that is used to model any steel object. The idea is that one or several point dipoles have the same magnetization as a naval ship, inducing the same disturbance.

Suppose we have a steel object Ω at location $\mathbf{d}$ and we observe the magnetic field around Ω from location $\mathbf{r}$, also the sensor location. We can define these positions as vectors in $\mathbb{R}^3$:

$$\mathbf{r} := \mathbf{r}(x, y, z) \quad \text{and} \quad \mathbf{d} := \mathbf{d}(x, y, z)$$

We define $\hat{\mathbf{r}}$ as the difference vector in $\mathbb{R}^3$, between $\mathbf{r}$ and $\mathbf{d}$. In Figure 2.1 a figure can be found that shows the relation between $\mathbf{r}, \mathbf{d}$ and $\hat{\mathbf{r}}$. A magnetic point dipole also has a magnetic moment $\mathbf{m}$. The magnetic moment of the point dipole in the x, y and z-direction is given by

$$\mathbf{m} := \mathbf{m}(x, y, z)$$

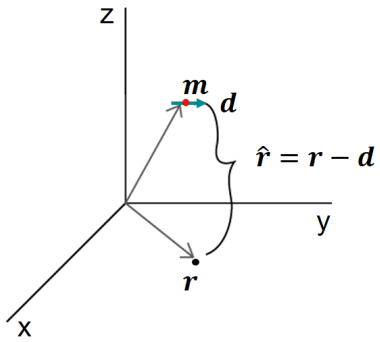

Figure 2.1: The red dot represents a steel object Ω

We define the magnetic field strength $\mathbf{H}$ and magnetic induction field $\mathbf{B}$ at location $\mathbf{r}(x, y, z)$ as vectors in $\mathbb{R}^n$.

$$\mathbf{H} := \mathbf{H}(\mathbf{r}) \quad \text{and} \quad \mathbf{B} := \mathbf{B}(\mathbf{r})$$

A summary of the symbols defined can be found in the Table 2 .

$\mathbf{H}$	is the magnetic field strength in ampères per meter	[A/m]
	This field is often referred to as the *magnetic field*, as was done in chapter one.	
$\mathbf{B}$	is the magnetic induction field in tesla	[T]
	This field is also often referred to as the *magnetic field*.	
$\mathbf{d}$	represents the location of the steel object Ω (i.e., the ship), in meters	[m].
$\mathbf{r}$	is the sensor location in meters	[m]
$\hat{\mathbf{r}} = \mathbf{r} - \mathbf{d}$	is the vector difference of the sensor and ship location	[m]
$\mathbf{m}$	represents the magnetic moment of a steel object	
	and it is given in ampéres squared meter	[Am^2]

Table 2.1: Symbols used to define the current situation.

When we measure a magnetic field with a sensor, we do not immediately obtain the $\mathbf{H}$-field. We obtain the magnetic induction field $\mathbf{B}$. Therefore, an important equality that we use is

$$\mathbf{B} = \mu_0 \mathbf{H} \tag{2.1}$$

Why we are allowed to assume the equality (2.1), will be explained in the next part of this chapter. Now to get back to the physics and the goal of this project, the goal is to find the magnetic background field. Because the magnetic background field is assumed to be locally uniform, the magnetic background field is given by

$$\mathbf{H}_0(\mathbf{r}) = \mathbf{H}_0$$

However, a measurement obtains the $\mathbf{B}$-field, so we will use $\mathbf{B}_0$ in the future, as the background field we are looking for. We denote the total field that is actually measured on board by $\mathbf{B}$. Recall that the magnetic distortion field or magnetic signature is the magnetic field induced by a disturber Ω, hence, we will denote the magnetic distortion field at location $\mathbf{r}$ by

$$\mathbf{B}_\Omega(\mathbf{r})$$

In order to construct a successful model, we disregarded considering the steel of a large naval vessel. We started by looking at smaller magnetic objects first. In this chapter we imagine a little piece of steel. Hence, suppose we do not have a large ship behaving as a magnet, but suppose we have a single point, a *magnetic dipole*. A dipole is a point containing two poles, north and south, often used to model small magnetic objects, such as magnets. A point dipole has volume that approaches zero, unlike a volume dipole. A magnetic dipole has a magnetic moment $\mathbf{m}$ and therefore a magnetic induction field $\mathbf{B}$ around it, just like our naval vessels. We start by computing the magnetic induction field $\mathbf{B}$ of one dipole, after which we look at more dipoles. More dipoles give us more variety in $\mathbf{B}$, which allows us to model the $\mathbf{B}$-field for a ship more accurately. Considering this, the red dot in Figure 2.1 can be considered a dipole.

The magnetic induction field at some location $\mathbf{r}$ of a point dipole at the origin is given by

$$\mathbf{B}(\mathbf{r}) = \frac{\mu_0}{4\pi}\left[\frac{3(\mathbf{m}\cdot\mathbf{r})\mathbf{r}}{\|\mathbf{r}\|^5} - \frac{\mathbf{m}}{\|\mathbf{r}\|^3}\right] \tag{2.2}$$

where $\mathbf{d}$ is the location of the dipole, $\mathbf{m}$ is its magnetic moment and $\mathbf{r}$ is the observation point of the magnetic induction field (e.g., a sensor location).

We have come to this equation by deriving the magnetic induction field $\mathbf{B}$ using the *Maxwell Equations*. Instead of starting with a point dipole, we have derived $\mathbf{B}$ for a three dimensional magnetic rod, a volume dipole, and by subsequently shrinking its volume to a point dipole, without changing its magnetic moment. In the limit, what remains is the magnetic dipole.

2.1 Maxwell's Equations

It all starts with Maxwell's equations, the origin of all electromagnetic theory and modeling [6]. So before we can start any work on deriving the magnetic induction field $\mathbf{B}$ for a dipole, we have to look at Maxwell's equations.

James Clerk Maxwell was a Scottish physicist and mathematician who published an early form of the Maxwell's equations around 1860 [6].

The equations are given in differential form by

$$\begin{cases} \nabla \cdot \mathbf{D} = \rho \\ \nabla \cdot \mathbf{B} = 0 \\ \nabla \times \mathbf{E} = -\frac{\partial \mathbf{B}}{\partial t} \\ \nabla \times \mathbf{H} = \mathbf{J} + \frac{\partial \mathbf{D}}{\partial t} \end{cases}$$

where $\mathbf{D}$ is the electric flux density in coulomb per meter^2 [C/m^2] and $\mathbf{E}$ is the intensity of the electric field in volts per meter [V/m]. The electric current density is given by $\mathbf{J}$ in units of ampères per meter^2 [A/m^2] and ρ is electric charge density in coulombs per meter^3 [C/m^3].

Maxwell's equations are based on the following laws in the next section.

2.1.1 Gauss' Law

The first two Maxwell equations are Gauss' Law written in differential form.

$\nabla \cdot \mathbf{D} = \rho$ states that electrical charges produce an electric field

$\nabla \cdot \mathbf{B} = 0$ states that there are no magnetic mono poles

2.1.2 Faraday's Law

$$\nabla \times \mathbf{E} = -\frac{\partial \mathbf{B}}{\partial t}$$

This equation is actually called the Maxwell-Faraday equation and it is a modification and generalization of Faraday's Law. This law states that electric fields are produced by changing magnetic fields.

2.1.3 Ampère's Law

$$\nabla \times \mathbf{H} = \mathbf{J} + \frac{\partial \mathbf{D}}{\partial t}$$

The last equation is the differential form of Ampère's Law. It states that magnetic fields are the result from currents and changing electric fields.

2.1.4 Magnetostatic form of Maxwell's equations

Earth's magnetic field and magnetic fields of naval vessels change very slowly in time, so we may consider them static in nature. Because of this, we can ignore the time dependence and induced electric fields in Maxwell's equations. So we use Gauss' Law and Ampère's Law where $\mathbf{J} \equiv \mathbf{0}$. We also ignore $\frac{\partial}{\partial t}$ and the density of electric charges ρ. We get a new set of equations under this current-free condition to describe the static magnetic field, given by

$$\begin{cases} \nabla \cdot \mathbf{B} = 0 \\ \nabla \times \mathbf{H} = \mathbf{0} \end{cases} \tag{2.3}$$

We can use these equations to describe the current-free problem and derive a solution.

2.1.5 Current-free problem

Solving this current-free problem means that we will determine the magnetic induction field $\mathbf{B}$, that is produced by some magnetization $\mathbf{M}$. In this section we will solve the current-free problem, given by

$$\begin{cases} \nabla \cdot \mathbf{B} = 0 \\ \nabla \times \mathbf{H} = \mathbf{0} \\ \mathbf{B} = \mu_0(\mathbf{H} + \mathbf{M}) \end{cases} \tag{2.4}$$

Here, $\mu_0 = 4\pi \cdot 10^{-7}$ henries per meter [H/m] is the magnetic permeability in everywhere in $\mathbb{R}^3$. The relation $\mathbf{B} = \mu_0(\mathbf{H} + \mathbf{M})$ in (2.4) holds for every location in vacuum, inside a steel object. When outside of a vacuum space, $\mathbf{M} = 0$. The resulting relation

$$\mathbf{B} = \mu_0 \mathbf{H} \tag{2.5}$$

holds for every location $\mathbf{r}$ on a steel object Ω in $\mathbb{R}^3$ (see also equation (2.1)). Because we consider the magnetic fields outside a steel object, we use the equality (2.5) , where $\mathbf{M} = 0$.

Because $\nabla \times \mathbf{H} = \mathbf{0}$, there exists a magnetic scalar potential φ such that

$$\mathbf{H} = -\nabla\varphi \tag{2.6}$$

Combining the equations in (2.4) and and the potential (2.6), we find:

$$\nabla \cdot \mu_0(\mathbf{H} + \mathbf{M}) = 0 \tag{2.7}$$

Using the linearity of the divergence operator, we can rewrite this as followed

$$\mu_0(\nabla \cdot \mathbf{H} + \nabla \cdot \mathbf{M}) = 0 \tag{2.8}$$

$$\nabla \cdot \mathbf{H} = -\nabla \cdot \mathbf{M} \tag{2.9}$$

It follows from equation 2.6 that $\nabla \cdot (\nabla\varphi) = \nabla \cdot \mathbf{M}$ resulting in

$$\Delta\varphi = \nabla \cdot \mathbf{M} \tag{2.10}$$

As $\Delta\varphi$ describes the change or generation of magnetic charges, which induces a magnetic field, we can assume $\nabla \cdot \mathbf{M}$ is the source of the magnetic induction field $\mathbf{B}$. Note that equation (2.10) is of the form

$$\Delta u = f$$

This is a non-homogeneous Poisson equation. Suppose there is a Φ such that $\Delta\Phi = \delta_0$. We find that the solution u is given by the convolution between Green's function for the Laplace operator in $\mathbb{R}^3$ and the source $\nabla \cdot \mathbf{M}$ and so

$$u(\mathbf{r}) = \iiint_{\mathbb{R}^3} \Phi(\mathbf{r} - \mathbf{r}')f(\mathbf{r}')dr' \qquad \text{, with } \Phi(\mathbf{x}) = -\frac{1}{4\pi}\frac{1}{\|\mathbf{x}\|}$$

With $\Phi(\mathbf{x})$ being Green's function for the Laplace operator in $\mathbb{R}^3$. We apply the equation above to equation (2.10) and we find that the potential for any magnetization in $\mathbb{R}^3$ becomes

$$\varphi(\mathbf{r}) = -\frac{1}{4\pi}\iiint_{\mathbb{R}^3} \frac{1}{||\mathbf{r} - \mathbf{r}'||}\nabla' \cdot \mathbf{M}(\mathbf{r}')d\mathbf{r}' \tag{2.11}$$

We will use this potential later on.

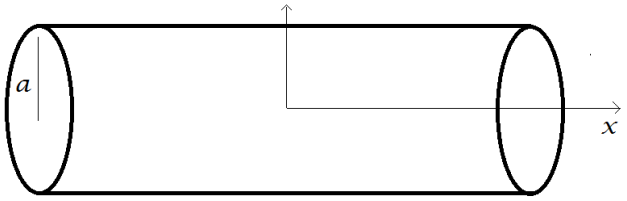

Figure 2.2: The three-dimensional rod Ω

2.2 A three-dimensional rod

Using circle-cylindrical coördinates (x, ρ, φ), suppose we have a rod of length 2ℓ, a radius a and a magnetization in the x-direction. Denote the rod by Ω.

The magnetization in the x-direction, only exists inside the rod. So we use a Heaviside-function $U(x)$ to define:

$$\mathbf{M} = \frac{M_0}{\mathsf{Vol}(\Omega)}\mathbf{u}_x \left[U(x+\ell) - U(x-\ell)\right] U(a-\rho) \tag{2.12}$$

Note that $\mathbf{M} = \mathbf{0}$ everywhere outside the rod.

The magnetic dipole moment of the rod is obtained by integrating $\mathbf{M}$ over the entire volume.

$$\begin{aligned}
\mathbf{m} = \iiint_{V_\infty} \mathbf{M} dV &= \int_{x=-\infty}^{\infty}\int_{\rho=0}^{\infty}\int_{\varphi=0-\infty}^{2\pi} \frac{M_0}{\mathsf{Vol}(\Omega)}\mathbf{u}_x \left[U(x+\ell) - U(x-\ell)\right] U(a-\rho) dx \cdot d\rho \cdot d\varphi \\
&= \frac{M_0}{\mathsf{Vol}(\Omega)}\mathbf{u}_x \cdot \int_{x=-\infty}^{\infty} \left[U(x+\ell) - U(x-\ell)\right] dx \cdot \int_{\rho=0}^{\infty} U(a-\rho) \cdot \rho d\rho \cdot \int_{\varphi=0}^{2\pi} d\varphi \\
&= \frac{M_0}{\mathsf{Vol}(\Omega)}\mathbf{u}_x \cdot 2\ell \cdot \int_{\rho=0}^{a} \rho d\rho \cdot 2\pi \\
&= \frac{M_0}{\mathsf{Vol}(\Omega)}\mathbf{u}_x \cdot 2\pi \cdot \ell \cdot a^2 = \frac{M_0}{\mathsf{Vol}(\Omega)}\mathbf{u}_x \cdot \mathsf{Vol}\Omega = M_0\mathbf{u}_x
\end{aligned} \tag{2.13}$$

Note that $\int_{\rho=0}^{a} \rho d\rho = \frac{1}{2}a^2$ and $2\pi\ell a^2$ is the volume of the magnetic rod Ω. Also observe that $\mathbf{m}$ is constant and independent of the dimensions of the rod Ω.

2.2.1 Shrinking the rod, part 1

Because we want to shrink the three-dimensional magnetic rod to a single point, we have to shrink some dimensions of the rod, part by part. We start by letting the radius a approach zero. Note that the magnetic dipole moment should stay the same. Therefore, if we shrink the volume of the rod, while keeping the same magnetic dipole moment, we have to increase the magnetization.

So suppose the magnetization of the shrunk rod, now a line, is

$$\mathbf{M} = c \cdot \mathbf{u}_x \left[U(x+\ell) - U(x-\ell)\right] \delta(y) \cdot \delta(z) \tag{2.14}$$

With δ a dirac delta and c a constant yet to be determined.

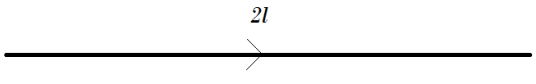

Figure 2.3: The three-dimensional rod, now a line

We are going to determine c such that the magnetic dipole moment of the line dipole and the magnetic rod are the same. By definition of the magnetic dipole moment, we find:

$$\begin{aligned}\mathbf{m} &= \iiint_{V_\infty} \mathbf{M} dV \\ &= \int_{x=-\infty}^{\infty}\int_{y=-\infty}^{\infty}\int_{z=-\infty}^{\infty} c\cdot\mathbf{u}_x\left[U(x+\ell)-U(x-\ell)\right]\delta(y)\delta(z)dx\cdot dy\cdot dz \\ &= c\cdot\mathbf{u}_x\cdot 2\ell\end{aligned} \tag{2.15}$$

Now choose $c = \frac{M_0}{\mathsf{Vol}(\Omega)}\pi a^2$ and we find that the magnetic dipole moment of the line is:

$$\begin{aligned}\mathbf{m} &= c\cdot\mathbf{u}_x\cdot 2\ell \\ &= \frac{M_0}{\mathsf{Vol}(\Omega)}\pi a^2\cdot\mathbf{u}_x\cdot 2\ell \\ &= M_0\mathbf{u}_x\end{aligned} \tag{2.16}$$

Note that this is the magnetic dipole moment for the three dimensional rod, see derivation (2.13).

2.2.2 The potential

To summarize what we have found so far, we look back for a little bit. We have found the potential φ such that $\mathbf{H} = -\nabla\varphi$, meaning we are able to calculate the magnetic field $\mathbf{H}$, or the magnetic induction field $\mathbf{B}$, see equation (2.5). However, we are not quite there yet. The potential that we have found holds for any magnetization in $\mathbb{R}^3$. But now we are going to look at the potential for a more specific situation: the potential for the magnetized rod.

We apply the potential given by equation (2.11) to the rod that has been shrunk to a line, we integrate over its entire volume, this gives us

$$\varphi(\mathbf{r}) = -\frac{1}{4\pi}\iiint_{V_\infty}\frac{1}{\|\mathbf{r}-\mathbf{r}'\|}(\nabla'\cdot\mathbf{M}')(\mathbf{r}')d\mathbf{r}' \tag{2.17}$$

We substitute the magnetization $\mathbf{M}$ in equation (2.14) with the constant c and do another few calculations. We find

$$\mathbf{M}' = M_0\pi a^2\mathbf{u}_x\cdot\left[U(x'+\ell)-U(x'-\ell)\right]\delta(y')\delta(z') \tag{2.18}$$

$$\nabla'\cdot\mathbf{M}' = \begin{pmatrix}\partial x'\\ \partial y'\\ \partial z'\end{pmatrix}\cdot\begin{pmatrix}M_x'\\ 0\\ 0\end{pmatrix} = \partial x'\cdot M_x' = M_0\pi a^2\left[\delta(x'+\ell)-\delta(x'-\ell)\cdot\delta(y')\delta(z')\right] \tag{2.19}$$

The equation for the scalar potential becomes:

$$\varphi(\mathbf{r}) = \frac{1}{4\pi}\cdot\int_{x'=-\infty}^{\infty}\int_{y'=-\infty}^{\infty}\int_{z'=-\infty}^{\infty}\frac{1}{\|\mathbf{r}-\mathbf{r}'\|}\cdot M_0\pi a^2[\delta(x'+\ell)-\delta(x'-\ell)]\cdot\delta(y')\cdot\delta(z')\cdot dx'dy'dz' \tag{2.20}$$

Note that the observation point is given by $\mathbf{r} = (x,y,z)$ and $\mathbf{r}' = (x',y',z')$. So we can rewrite the distance between the two

$$\varphi(\mathbf{r}) = -\frac{1}{4\pi}\cdot M_0\pi a^2\int_{x'=-\infty}^{\infty}\int_{y'=-\infty}^{\infty}\int_{z'=-\infty}^{\infty}\frac{[\delta(x'+\ell)-\delta(x'-\ell)]\cdot\delta(y')\cdot\delta(z')}{\sqrt{(x-x')^2+(y-y')^2+(z-z')^2}}\cdot dx'dy'dz' \tag{2.21}$$

By properties of the dirac delta function, we find the potential

$$\varphi(\mathbf{r}) = -\frac{1}{4\pi}M_0\pi a^2\left[\frac{1}{\sqrt{(x+\ell)^2+y^2+z^2}}-\frac{1}{\sqrt{(x-\ell)^2+y^2+z^2}}\right] \tag{2.22}$$

The derivation from equation (2.20) to (2.22) can be found in the appendix.

2.3 Shrinking the rod, part 2

We were able to calculate the potential of the magnetic line, using its magnetization. Its magnetization was derived from the magnetization of a rod. Now we want to shrink the line to a single point. We do this by letting its length ℓ approach zero, meanwhile increasing the magnetization so that the dipole moment remains the same.

To make things easier, we rewrite equation (2.22) such that letting ℓ approach zero is easy. For this, we use the definition of the central derivative of a function $f(x)$

$$f'(x) = \lim_{h\to 0} \frac{f(x+h) - f(x-h)}{2h}$$

We use this definition later on. We rewrite equation (2.22):

$$\begin{aligned} \varphi(\mathbf{r}) &= -\frac{1}{4\pi} M_0 \pi a^2 \left[\frac{1}{\sqrt{(x+\ell)^2+y^2+z^2}} - \frac{1}{\sqrt{(x-\ell)^2+y^2+z^2}} \right] \\ &= \frac{1}{4\pi} M_0 \pi a^2 \cdot 2\ell \cdot \frac{\frac{1}{\sqrt{(x+l)^2+y^2+z^2}} - \frac{1}{\sqrt{(x-l)^2+y^2+z^2}}}{2\ell} \end{aligned} \tag{2.23}$$

Recall that the magnetic dipole moment of the line is given by $m_x = M_0 \pi a^2$. So equation (2.23) becomes

$$\varphi(\mathbf{r}) = -\frac{1}{4\pi} m_x \cdot \frac{\frac{1}{\sqrt{(x+\ell)^2+y^2+z^2}} - \frac{1}{\sqrt{(x-\ell)^2+y^2+z^2}}}{2\ell} \tag{2.24}$$

This is where the definition of the derivative comes in. Let

$$f(x) = \frac{1}{\sqrt{x^2+y^2+z^2}} \tag{2.25}$$

and

$$f(x+\ell) = \frac{1}{\sqrt{(x+\ell)^2+y^2+z^2}} \tag{2.26}$$

$$f(x-\ell) = \frac{1}{\sqrt{(x-\ell)^2+y^2+z^2}} \tag{2.27}$$

Using this, we rewrite equation (2.23)

$$\varphi(\mathbf{r}) = -\frac{1}{4\pi} \mathbf{m} \cdot \frac{f(x+\ell) - f(x-\ell)}{2\ell} \tag{2.28}$$

Now let ℓ approach zero. Using equations afgeleide1, (2.26), (2.28) and the derivative of $f(x)$, we find

$$\begin{aligned} \varphi(\mathbf{r}) &= -\frac{1}{4\pi} \mathbf{m} \cdot \lim_{\ell\to 0} \frac{f(x+\ell) - f(x-\ell)}{2\ell} \\ &= -\frac{1}{4\pi} \mathbf{m} \cdot f'(x) \\ &= -\frac{1}{4\pi} \mathbf{m} \cdot -\frac{1}{2}(x^2+y^2+z^2)^{-\frac{3}{2}} \cdot 2x \\ &= -\frac{1}{4\pi} \mathbf{m} \cdot -\frac{x}{\|\mathbf{r}\|^3} \end{aligned} \tag{2.29}$$

Note that this is the potential for a line dipole, whose length ℓ is approaching zero, in other words a point dipole. Now we use

$$\mathbf{H} = -\nabla\varphi$$

to calculate the magnetic $\mathbf{H}$-field.

$$\begin{aligned} -\nabla\varphi &= -\nabla\left(\frac{1}{4\pi}\mathbf{m}\cdot-\frac{x}{\|\mathbf{r}\|}\right) \\ &= -\frac{1}{4\pi}\cdot\mathbf{m}\cdot\nabla\left(\frac{x}{\|\mathbf{r}\|}\right) \end{aligned} \tag{2.30}$$

And so we find, by using the partial derivatives

$$\mathbf{H} = -\frac{1}{4\pi}\cdot\mathbf{m}\cdot\left[\left(\frac{1}{\|\mathbf{r}\|^3}-3x^2\cdot\frac{1}{\|\mathbf{r}\|^5}\right)\mathbf{u}_x - 3xy\frac{1}{\|\mathbf{r}\|^5}\mathbf{u}_y - 3xz\cdot\frac{1}{\|\mathbf{r}\|^5}\mathbf{u}_z\right] \tag{2.31}$$

We take a look at what this derivation has achieved so far. We have found $\mathbf{H}$ of a dipole with magnetic moment $\mathbf{m} = M_0\pi a^2 2\ell\mathbf{u}_x$. Also, we used equation (2.25) and its derivative $f'(x)$ with respect to x, to let ℓ approach zero. We can generalize this result for a dipole with a magnetic moment

$$\mathbf{m} = m_x\mathbf{u}_x + m_y\mathbf{u}_y + m_z\mathbf{u}_z \tag{2.32}$$

And suppose

$$f(\mathbf{r}) = f(x,y,z) = \frac{1}{\|\mathbf{r}\|}$$

The potential with $f(\mathbf{r})$ is computed as followed:

$$\begin{aligned} \varphi(\mathbf{r}) &= \frac{1}{4\pi}(m_x f_x + m_y f_y + m_z f_x) \\ &= \frac{1}{4\pi}\left(m_x\cdot-\frac{x}{\|\mathbf{r}\|^3} + m_y\cdot-\frac{y}{\|\mathbf{r}\|^3} + m_z\cdot-\frac{z}{\|\mathbf{r}\|}\right) \\ &= -\frac{1}{4\pi}\frac{m_x\cdot x + m_y\cdot y + m_z\cdot z}{\|\mathbf{r}\|^3} \\ &= -\frac{1}{4\pi}\frac{\mathbf{m}\cdot\mathbf{r}}{\|\mathbf{r}\|^3} \end{aligned}$$

In conclusion, we find:

$$\varphi(\mathbf{r}) = -\frac{1}{4\pi}\frac{\mathbf{m}\cdot\mathbf{r}}{\|\mathbf{r}\|^3} \tag{2.33}$$

We can obtain $\mathbf{H}$ by using equation (2.6) :

$$\begin{aligned} \mathbf{H} &= -\nabla\left(\frac{\mathbf{m}\cdot\mathbf{r}}{4\pi\|\mathbf{r}\|^3}\right) \\ &= -\nabla\left(\mathbf{m}\cdot\frac{\mathbf{r}}{4\pi\|\mathbf{r}\|^3}\right) \end{aligned} \tag{2.34}$$

To make things a little easier to work with, we call

$$P = \mathbf{m} \quad \text{and} \quad Q = \frac{\mathbf{r}}{4\pi\|\mathbf{r}\|^3} \tag{2.35}$$

This results in

$$\begin{aligned} \mathbf{H} &= -\nabla(P\cdot Q) \\ &= -\left[(P\cdot\nabla)Q + (Q\cdot\nabla)P + P\times(\nabla\times Q) + Q\times(\nabla\times P)\right] \end{aligned} \tag{2.36}$$

Because $\mathbf{m}$ is not dependent on $\mathbf{r}$. it follows that $(Q\nabla)P, P\times(\nabla)$ and $Q\times(\times P)$ are zero and therefore

$$\mathbf{H} = -\left[(P\cdot\nabla)Q\right]$$

We find

$$\mathbf{H} = -\left[(P\cdot\nabla)Q\right] = \frac{1}{4\pi}\left[\frac{3(\mathbf{m}\cdot\mathbf{r})\mathbf{r}}{||\mathbf{r}||^5} + \frac{\mathbf{r}}{||\mathbf{r}||^3}\right]$$

In conclusion, for a point dipole at the origin we have

$$\mathbf{B}(\mathbf{r}) = \frac{\mu_0}{4\pi}\left[\frac{3(\mathbf{m}\cdot\mathbf{r})\mathbf{r}}{\|\mathbf{r}\|^5} - \frac{\mathbf{m}}{\|\mathbf{r}\|^3}\right] \quad \text{or} \quad \mathbf{B}(\mathbf{r}) = \frac{\mu_0}{4\pi}\left[\frac{3(\mathbf{m}\cdot\mathbf{r})\mathbf{r}}{\|\mathbf{r}\|^5} - \frac{\mathbf{m}}{\|\mathbf{r}\|^3}\right] \tag{2.37}$$

We can generalize the solution in (2.37) for a dipole that located anywhere in $\mathbb{R}^3$. We consider the dipole position $\mathbf{d}$:

$$\mathbf{B}(\mathbf{r}) = \frac{\mu_0}{4\pi}\left[\frac{3(\mathbf{m}\cdot\hat{\mathbf{r}})\hat{\mathbf{r}}}{\|\hat{\mathbf{r}}\|^5} - \frac{\mathbf{m}}{\|\hat{\mathbf{r}}\|^3}\right] \tag{2.38}$$

where $\hat{\mathbf{r}} = \mathbf{r} - \mathbf{d}$.

Chapter 3

A model for determining of the magnetic background field

Now that we know more about magnetic dipoles, and that their field is dependent on the magnetic moment $\mathbf{m}$ and position $\mathbf{r}$, we can start looking at our goal.

The goal is to determine the magnetic background field $\mathbf{H}_0$ at some location $\mathbf{r}$ at sea. Note that magnetic sensors do not measure the $\mathbf{H}$-field, but the magnetic induction field $\mathbf{B}$. Therefore, we speak of measuring $\mathbf{B}$ and determining the magnetic background field $\mathbf{B}_0$. Recall that when on board at sea, the sensors do not just measure $\mathbf{B}_0$, making the task much more of a challenge. We actually measure a total field $\mathbf{B}$. This measured field is a combination of the magnetic background field and other magnetic fields that are induced by various steel objects. We define the following symbols:

$\mathbf{B}$	is the total magnetic field measured at location, in tesla $\mathbf{r}$	[T]
$\mathbf{B}_0$	is the magnetic background field to be determined in tesla	[T]
Ω	is a steel object that induces a magnetic field	
$\mathbf{B}_\Omega$	is the magnetic field induced by the steel object Ω in tesla	[T].

Table 3.1: The symbols used to define the model.

With these symbols, we can say that the total field that is measured at location $\mathbf{r}$ is given by

$$\mathbf{B} := \mathbf{B}_0 + \mathbf{B}_{\Omega_1} + \mathbf{B}_{\Omega_2} + ... + \mathbf{B}_{\Omega_n} \tag{3.1}$$

Where $\Omega_1, \Omega_2, ..., \Omega_n$, with n a finite number are n steel objects. For the topic of our research, we can imagine the steel of a naval vessel, the steel of the coils of its degaussing system and other steel objects on board to be among these n steel objects. Because we can not keep track of the magnetic field of every steel object on board, we simply define the total magnetic field at location $\mathbf{r}$ as

$$\mathbf{B}(\mathbf{r}) = \mathbf{B}_0 + \mathbf{B}_\Omega \tag{3.2}$$

Where $\mathbf{B}_\Omega$ is the magnetic field induced by all the steel of and in a naval ship. Looking at equation (3.2), we see that if we know the total field $\mathbf{B}$ and the magnetic field induced by Ω, that is $\mathbf{B}_\Omega$, we can determine the magnetic background field $\mathbf{B}_0$. The total field $\mathbf{B}$ is something we can measure with the use of sensors. Currently, the Royal Dutch Navy uses only one sensor for this. This prediction model will use a sensor array to obtain measurement data. For the other field, $\mathbf{B}_\Omega$, we model the naval ship with one or several dipoles and we use the prediction model to compute $\mathbf{B}_\Omega$. If we were to model the naval ship Ω with just one dipole, we can calculate $\mathbf{B}_\Omega$ analytically with the expression for the dipole we derived in the previous chapter.

The image below illustrates the idea behind modeling a ship with a dipole in the x, y and z plane. This chapter further explains the concept of the prediction model and how it came about.

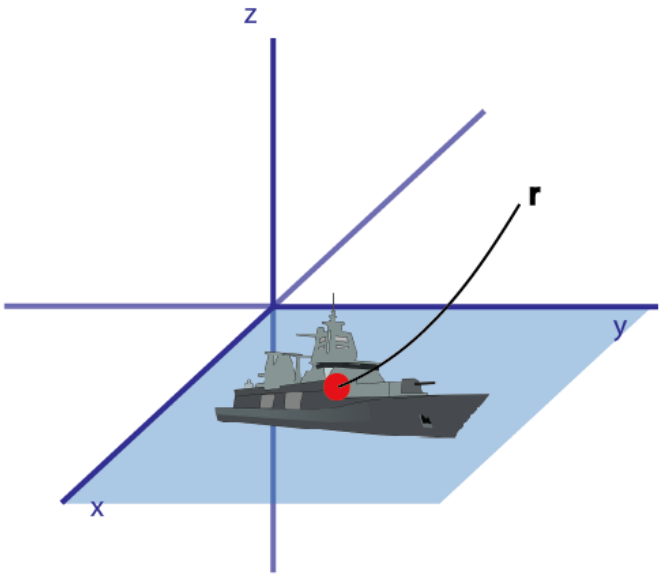

Figure 3.1: A ship at sea at location $\mathbf{r}(x, y, z)$

3.1 The concept

Today, measurements of the background field at sea are done by equipping the mast with a single sensor, see Figure 3.2. This sensor measures the magnetic field around the mast and assumes this field to be solely the magnetic background field $\mathbf{B}_0$ we are looking for. As explained in chapter 1, this magnetic background field is then used for degaussing the magnetic signature of the vessel, which needs the proper information of $\mathbf{B}_0$. However, the magnetic field that is measured by the single sensor in the mast, presumably $\mathbf{B}_0$, might still consist of more than just the original background field. In other words, the sensor in the mast might still measure the magnetic field induced by the steel of the ship.

Figure 3.2: The Zr.Ms. Van Amstel (1993) imagined with a measure location in the mast.

Figure 3.2 also encourages this intuition, because we see that the sensor in the mast, is close to a lot steel, namely the vessel it self. These are also realistic proportions as the Zr.Ms. Van Amstel is a frigate, a typical object on which a sensor array could be implemented.

The concept of our new method is that, apart from determination of the magnetic background field, we try to enhance the accuracy of the measurements, by doing more than a single measurement. We do this by arranging multiple sensors in the mast to create a sensor array, see Figure 3.3, and see if there is any added value to higher the amount of sensors in the mast.

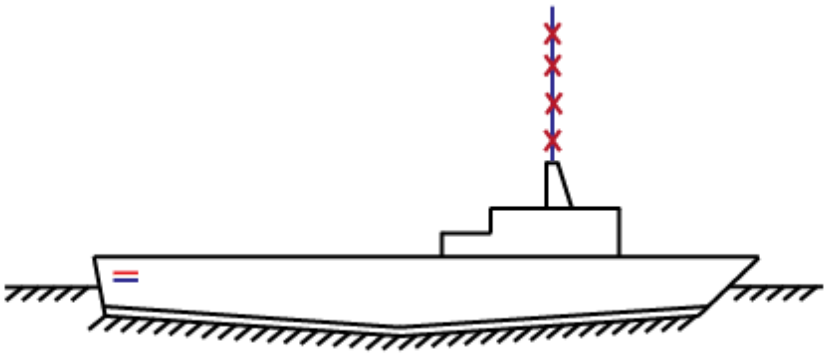

Figure 3.3: An array of sensors in the mast.

3.2 From a naval vessel to a single point

As we did in chapter 2, we do not consider shape of a naval vessel. We assume the magnetic field of a naval vessel can be modeled by multiple magnetic dipoles. We view the surface of the ocean as the x, y-plane, see Figure 3.1. We start with measuring the magnetic field in the x, y-plane containing one dipole. Later we increase the number of dipoles mimicking the disturbance of a naval vessel. See Figure 3.4d.

3.3 An expression for the magnetic field of a dipole

In the previous section we derived an expression for the magnetic field $\mathbf{H}$ of a dipole. However, as mentioned earlier this chapter, the sensors measure the magnetic field $\mathbf{B}$. Therefore, instead using the dipole expression for $\mathbf{H}$, we use an expression for $\mathbf{B}$. Using the following important equality, explained in section 2.4

$$\mathbf{B} = \mu_0 \mathbf{H} \tag{3.3}$$

We use the following expression for $\mathbf{B}$:

$$\mathbf{B}(\mathbf{m}, \mathbf{r}) = \frac{\mu_0}{4\pi} \left[\frac{3(\mathbf{m} \cdot \mathbf{r})\mathbf{r}}{\|\mathbf{r}\|^5} - \frac{\mathbf{m}}{\|\mathbf{r}\|^3} \right] \tag{3.4}$$

We use this expression in defining the magnetic field $\mathbf{B}_\Omega$ induced by steel object Ω or dipole .

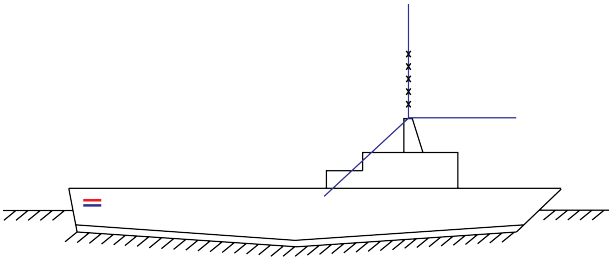

(a) A ship with sensors along the z-axis

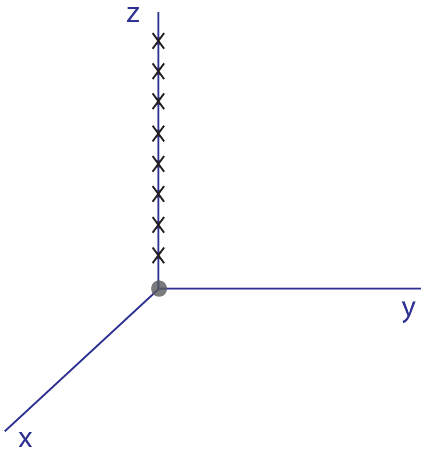

(b) Modeling a naval vessel as a single dipole in the x, y-plane

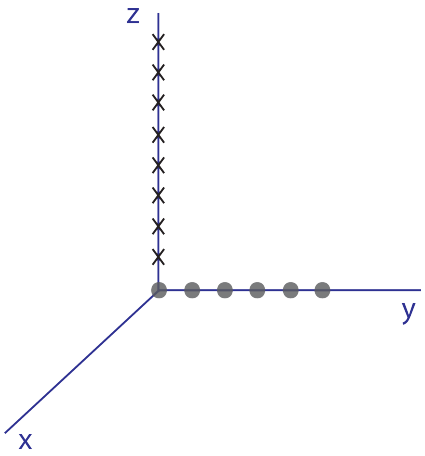

(c) Increasing the number of dipoles to N

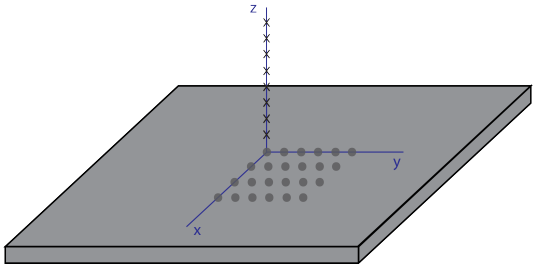

(d) Modeling a steel object Ω with multiple dipoles

Figure 3.4: Modeling a steel object Ω by multiple dipoles

3.4 The prediction model

Recall that the concept of the prediction model revolves around solving

$$\mathbf{B} = \mathbf{B}_0 + \mathbf{B}_\Omega \quad \text{for} \quad \mathbf{B}_0.$$

The model that we formulated to determine the background field is based on forward and inverse modeling. We start by solving a forward problem followed by solving the inverse problem.

By forward, we mean, if $\mathbf{B}_0$ and the sources in Ω are apriori known, then we can forwardly calculate calculate the $\mathbf{B}$-field using the expression for the dipole, a complete formulation can be found in the next chapter. The forward problem results in the magnetic field $\mathbf{B}$ at location $\mathbf{r}$.

By solving the inverse problem, we mean that we predict $\mathbf{B}_\Omega$, and in particular $\mathbf{B}_0$ from the forward computed $\mathbf{B}$-field at location $\mathbf{r}$. $\mathbf{B}$. We are interested in the solution $\mathbf{B}_0$, therefore we concentrate on a formulation of the inverse problem. If we know how to solve the inverse problem, then we have a our prediction model.

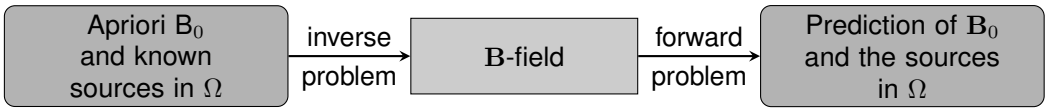

Figure 3.5: The relation between the forward and inverse problem.

Simulations use both the forward and the inverse problem. In chapter 8 we test the prediction model on simulated data. This data is not measured by sensors, but simulated by apriori defining $\mathbf{B}_0$ and the sources in Ω and solving the forward problem. Afterwards, the simulation experiment determines the magnetic background field $\mathbf{B}_0$ with the prediction model.

In reality, we do not solve the forward problem. The sources in Ω are not apriori known, and we use measurements via the sensor array to obtain the (total) $\mathbf{B}$-field at location $\mathbf{r}$, resulting in a data set we can use for the prediction model. Therefore, we can visualize the model in a flow chart, see Figure 3.6.

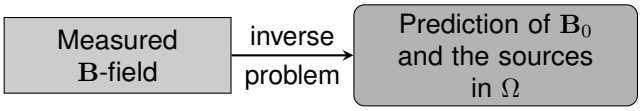

Figure 3.6: The prediction model

Recall that this research also determines if the use of the sensor array for obtaining data has any added value to the approximated $\mathbf{B}_0$, in comparison to obtaining data with one sensor. Note that if the true magnetic background field $\mathbf{B}_0$ and the prediction of $\mathbf{B}_0$ do not differ from each other too much, we have a successful model that determines $\mathbf{B}_0$ accurately using measured data $\mathbf{B}$. The prediction model consists of the last two blocks of the flow chart in Figure 3.5. To visualize how the prediction model works, see Figure 3.6.

To keep notation consistent, consider the following symbols:

$\mathbf{B}_0$	the magnetic background field that is to be determined	[T]
$\mathbf{B}_0^c$	the approximation of $\mathbf{B}_0$, determined with the prediction model	[T]
$\mathbf{B}_\Omega$	the magnetic field around object Ω	[T]

Table 3.2: Symbols used to define the forward problem.

Chapter 4

The forward problem

When looking at what our model is supposed to do, the forward problem should satisfy the following:

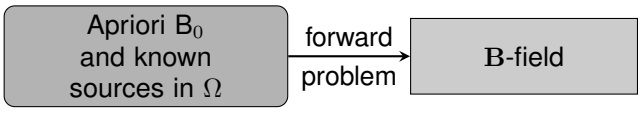

Figure 4.1: The forward problem.

To formulate the forward problem, we consider the magnetic field of N dipoles $\mu_1, \mu_2, ..., \mu_N$ instead of considering the magnetic field of a steel object Ω. Therefore, we use the expression of the magnetic point dipole as derived in chapter 2, as followed:

$$\mathbf{B}_\Omega = \mathbf{B}_{\mu_1} + \mathbf{B}_{\mu_2} + ... + \mathbf{B}_{\mu_N} \tag{4.1}$$

We use equation (4.1) to formulate the forward problem.

The forward problem. *Given a uniform background field $\mathbf{B}_0$, magnetic dipoles $\mu_1, \mu_2, ..., \mu_N$ with positions $\mathbf{d}_1, \mathbf{d}_2, ..., \mathbf{d}_N$ and magnetic moments $\mathbf{m}_1, \mathbf{m}_2, ..., \mathbf{m}_N$. For N dipoles, calculate the magnetic induction field $\mathbf{B}$ in locations $\mathbf{r}_j$, with $j = 1, ..., M$:*

$$\mathbf{B}(\mathbf{r}_j) = \mathbf{B}_0 + \sum_{i=1}^{N} \frac{\mu_0}{4\pi} \left[\frac{3(\mathbf{m}_i \cdot \hat{\mathbf{r}}_{ij})\hat{\mathbf{r}}_{ij}}{\|\hat{\mathbf{r}}_{ij}\|^5} - \frac{\mathbf{m}_i}{\|\hat{\mathbf{r}}_{ij}\|^5} \right] \tag{4.2}$$

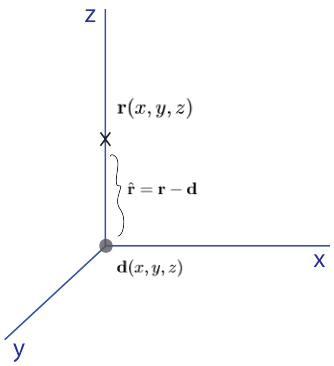

Figure 4.2: An example of a sensor denoted at location $\mathbf{r}$ measuring the magnetic field with a single dipole at the origin

In the formulation of the forward problem, we use equation (3.2) that states that the magnetic field at location $\mathbf{r}$ is given by

$$\mathbf{B}(\mathbf{r}) = \mathbf{B}_0 + \mathbf{B}_\Omega$$

.

Table 4 enlightens the symbols used in equation (4.2).

$\mathbf{B}(\mathbf{r}_j)$	the magnetic induction field at location $\mathbf{r}_j$, with $j \in \{1, .., M\}$	[T]
$\mathbf{B}_0$	the magnetic background field	[T]
μ_i	one out of N dipoles	
$\mathbf{B}_{\mu_i}$	the magnetic field induced by dipole μ_i	[T]
$\mathbf{d}_i$	represents the location of the i^{th} dipole	[m]
$\mathbf{m}_i$	represents the magnetic moment of the i^{th} dipole	[A·m^2]
$\mathbf{r}_j$	sensor location $j < M$	[m]
$\hat{\mathbf{r}}_{ij} = \mathbf{r}_j - \mathbf{d}_i$	the vector difference of the j^{th} sensor and i^{th} dipole location	[m]

Table 4.1: Symbols used to define the forward problem.

When modeling a steel object Ω with a dipole, the forward problem computes the $\mathbf{B}$-field of object Ω by computing $\mathbf{B}_{\mu_i}$ of dipole μ_i, with $j \in \{1, 2, ..., N\}$. We suppose the true fields $\mathbf{B}_0$ and $\mathbf{d}_i$ and $\mathbf{m}_i$ are fixed. Consider $\mathbf{B}_0$ first.

4.1 The magnetic background field B_0

To solve the forward problem, we will define $\mathbf{B}_0$ as earth's true magnetic background field and expect the solution of the inverse problem to return the same values for the approximation of $\mathbf{B}_0^{\varepsilon}$. The strength of the earth's magnetic background field varies between 25 and 65 microteslas μT (10^{-6}T) [8], we can use a value between 25 and 65 for an experiment later on. Consider $\mathbf{B}_0$ below.

$$\mathbf{B}_0 = \begin{bmatrix} B_x \\ B_y \\ B_z \end{bmatrix} \tag{4.3}$$

4.2 The magnetic field B_i of the dipole μ_i

Now consider $\mathbf{B}_{\mu_i}$. In this forward problem, we previously stated that we fix the sources in μ_i in advance. We know from chapter 2 and equation (3.4) that $\mathbf{B}_{\mu_i}$ is dependent on $\mathbf{m}_i$ and sensor location $\mathbf{r}_j$ and

$$\mathbf{B}_{\mu_i}(\mathbf{r}_j) = \frac{\mu_0}{4\pi}\left[\frac{3(\mathbf{m}_i \cdot \hat{\mathbf{r}}_{ij})\hat{\mathbf{r}}_{ij}}{\|\hat{\mathbf{r}}_{ij}\|^5} - \frac{\mathbf{m}_i}{\|\hat{\mathbf{r}}_{ij}\|^3}\right]$$

Where $\hat{\mathbf{r}}_{ij} = \mathbf{r}_j - \mathbf{d}_i$. Here, $\mathbf{r}_j$ is the location of the sensor j, in other words, the location of our measuring point and $\mathbf{d}_i$ is the position of the dipole μ_i. Using equation (3.4) we can calculate $\mathbf{B}_i$ by defining $\mathbf{m}_i$ and $\mathbf{d}_i$ in advance as the "true" magnetic moment and dipole position.

4.2.1 A fixed location d of the dipole

So for the forward problem, the total magnetic field $\mathbf{B}(\mathbf{r}_j)$ at sensor location $\mathbf{r}_j$ is not measured with sensors, but calculated using $\mathbf{B}_i$, that is dependent on the fixed magnetic moment and fixed dipole location, and $\mathbf{B}_0$. We have to solve the following to determine $\mathbf{B}(\mathbf{r}_j)$:

$$\mathbf{B}_0 + \mathbf{B}_{\mu_i} = \mathbf{B}(\mathbf{r}_j) \tag{4.4}$$

This is equivalent to:

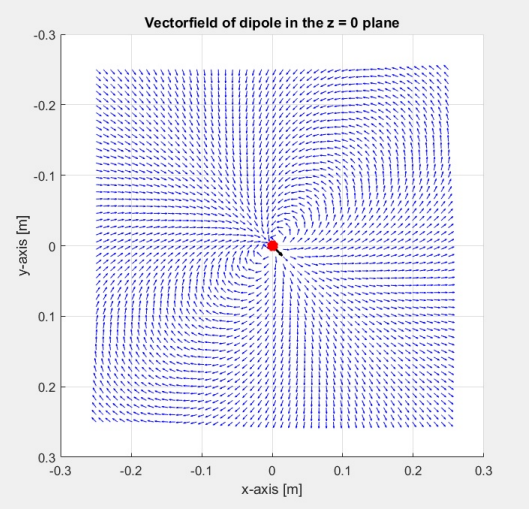

Figure 4.3: The magnetic field of a dipole at the origin

$$\begin{bmatrix} \mathbf{B}_x \\ \mathbf{B}_y \\ \mathbf{B}_z \end{bmatrix} + \frac{\mu_0}{4\pi}\left[\frac{3(\mathbf{m}_i \cdot \hat{\mathbf{r}}_{ij})\hat{\mathbf{r}}_{ij}}{\|\hat{\mathbf{r}}_{ij}\|^5} - \frac{\mathbf{m}_i}{\|\hat{\mathbf{r}}_{ij}\|^3}\right] \tag{4.5}$$

It is easy to calculate $\mathbf{B}(\mathbf{r}_j)$ if $\mathbf{m}_i$ and $\hat{\mathbf{r}}_{ij}$ are known. In this problem, they are, as the forward problem apriori fixes $\mathbf{m}_i$ and $\mathbf{d}_i$. The next step is to formulate and solve the inverse of the problem.

So inversely, suppose $\mathbf{B}(\mathbf{r}_j)$ is known, and we want to calculate $\mathbf{B}_i$. Because $\hat{\mathbf{r}}_{ij} = \mathbf{r}_j - \mathbf{d}_i$ with both $\mathbf{d}_i$ and $\mathbf{m}_i$ unknown, it becomes a lot harder to solve for $\mathbf{B}_i$. Especially if we were to do more than one measurement. Which we will, because we do N measurements along a naval ship's mast. For example, if we do M measurements and obtain $\mathbf{B}(\mathbf{r}_1), \mathbf{B}(\mathbf{r}_2), ..., \mathbf{B}(\mathbf{r}_M)$, and we place one dipole in vicinity of the sensors with magnetic moment $\mathbf{m}$ unknown and $\mathbf{B}_0$ is known, we get the nonlinear system:

$$\begin{cases} \mathbf{B}(\mathbf{r}_1) = \mathbf{B}_0 + \frac{\mu_0}{4\pi}\left[\frac{3(\mathbf{m}_i\cdot\hat{\mathbf{r}}_1)\hat{\mathbf{r}}_1}{\|\hat{\mathbf{r}}_1\|^5} - \frac{\mathbf{m}_i}{\|\hat{\mathbf{r}}_1\|^3}\right] \\ \mathbf{B}(\mathbf{r}_2) = \mathbf{B}_0 + \frac{\mu_0}{4\pi}\left[\frac{3(\mathbf{m}_i\cdot\hat{\mathbf{r}}_2)\hat{\mathbf{r}}_2}{\|\hat{\mathbf{r}}_2\|^5} - \frac{\mathbf{m}_i}{\|\hat{\mathbf{r}}_2\|^3}\right] \\ \mathbf{B}(\mathbf{r}_3) = \mathbf{B}_0 + \frac{\mu_0}{4\pi}\left[\frac{3(\mathbf{m}_i\cdot\hat{\mathbf{r}}_3)\hat{\mathbf{r}}_3}{\|\hat{\mathbf{r}}_3\|^5} - \frac{\mathbf{m}_i}{\|\hat{\mathbf{r}}_3\|^3}\right] \\ \vdots \\ \mathbf{B}(\mathbf{r}_M) = \mathbf{B}_0 + \frac{\mu_0}{4\pi}\left[\frac{3(\mathbf{m}_i\cdot\hat{\mathbf{r}}_M)\hat{\mathbf{r}}_M}{\|\hat{\mathbf{r}}_M\|^5} - \frac{\mathbf{m}_i}{\|\hat{\mathbf{r}}_1\|^3}\right] \end{cases} \tag{4.6}$$

For this reason, we disregard the unknown dipole location in this project. We choose a fixed location for the dipole. This makes the system linear in $\mathbf{m}$, which is obviously easier to solve.

4.3 Solving the forward problem

In conclusion, we define $\mathbf{B}_0$ and $\mathbf{B}_{\mu_i}$ to calculate $\mathbf{B}(\mathbf{r}_j)$. Solving the forward problem is easy, as we simply put in the predefined values, which returns a vector $\mathbf{B}(\mathbf{r}_j)$, which is the total magnetic field at some location $\mathbf{r}_j$. This can be done analytically or using `MATLAB`. Examples with one and several dipoles and measurements will be shown later on.

Chapter 5

The inverse problem

We have formulated the forward problem, and we know how to solve it. In this section it is explained how we solve the inverse problem.

Recall the inverse problem given by Figure 5.1.

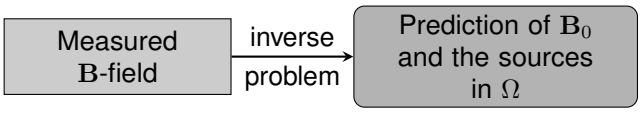

Figure 5.1: The prediction model

Instead of trying to calculate the magnetic field $\mathbf{B}$, it is known to us by the use of sensors. So we obtain $\mathbf{B}(\mathbf{r}_j)$ by measuring the magnetic field at location $\mathbf{r}_j$. The magnetic background field $\mathbf{B}_0$ and magnetic fields of the N dipoles $\mathbf{B}_{\mu_i}$, with $i = 1, 2, ..., N$, are now unknown instead.

5.1 A formulation of the inverse problem

The output of this model is the computed magnetic background field $\mathbf{B}_0^c$ and the calculated magnetic moment $\mathbf{m}^c$, on which $\mathbf{B}_{\mu_i}$ is dependent.

The inverse problem. *Given the measured induction field $\mathbf{B}(\mathbf{r}_j)$, known sensor positions $\mathbf{r}_j$ with $j = 1, 2, ..., M$ and known dipole positions $\mathbf{d}_i$, where $i = 1, 2, ..., N$. Find the magnetic background field $\mathbf{B}_0$ and magnetic moments $\mathbf{m}_i$, for $i = 1, 2, ..., N$.*

Here, $\mathbf{B}(\mathbf{r}_j)$ is a $(3M \times 1)$-vector, depending on the amount of measurements M.

5.2 The inverse problem as a linear system

Solving the inverse problem is a little bit more difficult than simply plugging in the measured values of the $\mathbf{B}$-field. Therefore, we reformulate the problem in such a way that it is easier to solve.

We know that the solution of the inverse problem has to result in $\mathbf{B}_0^c$ and $\mathbf{B}_{\mu_i}$. Let us start by rewriting what we know, see equation (3.2), the inverse problem should satisfy:

$$\mathbf{B}(\mathbf{r}_j) = \mathbf{B}_0^c + \mathbf{B}_{\mu_i} \tag{5.1}$$

Now we rewrite equation (5.1) such that we have a linear system, which is easier to solve. We start by considering one measurement and one dipole.

For one dipole with magnetic moment $\mathbf{m}$ and location $\mathbf{d}$, and for one measurement at location $\mathbf{r}$, we have

$$\mathbf{B}(\mathbf{r}) = \mathbf{B}_0^c + \frac{\mu_0}{4\pi}\left[\frac{3(\mathbf{m}\cdot\hat{\mathbf{r}})\hat{\mathbf{r}}}{\|\hat{\mathbf{r}}\|^5} - \frac{\mathbf{m}}{\|\hat{\mathbf{r}}\|^3}\right] \tag{5.2}$$

We can factor out the $\frac{1}{\|\hat{\mathbf{r}}\|^3}$, so now equation (5.2) is equivalent to

$$\mathbf{B}(\mathbf{r}) = \mathbf{B}_0^c + \frac{\mu_0}{4\pi\,\|\hat{\mathbf{r}}^3\|}\left[\frac{3(\mathbf{m}\cdot\hat{\mathbf{r}})\hat{\mathbf{r}}}{\|\hat{\mathbf{r}}\|^2} - \mathbf{m}\right] \tag{5.3}$$

We can rewrite the second term of the right hand side. Suppose

$$\hat{\mathbf{r}} = \mathbf{r} - \mathbf{d} = \begin{bmatrix} r_x \\ r_y \\ r_z \end{bmatrix} - \begin{bmatrix} d_x \\ d_y \\ d_z \end{bmatrix} = \begin{bmatrix} x \\ y \\ z \end{bmatrix}$$

This results in a (3×3)-matrix K which we use to define the inverse problem:

$$\mathbf{B}_{\mu_i} = \frac{\mu_0}{4\pi\,\|\hat{\mathbf{r}}\|^3}\left[\frac{3(\mathbf{m}\cdot\hat{\mathbf{r}})\hat{\mathbf{r}}}{\|\hat{\mathbf{r}}\|^2} - \mathbf{m}\right] = \frac{\mu_0}{4\pi\,\|\hat{\mathbf{r}}\|^3}\begin{bmatrix} \frac{3x^2}{\|\hat{\mathbf{r}}\|^2}\cdot m_x + \frac{3xy}{\|\hat{\mathbf{r}}\|^2}\cdot m_y + \frac{3xz}{\|\hat{\mathbf{r}}\|^2}\cdot m_z \\ \frac{3xy}{\|\hat{\mathbf{r}}\|^2}\cdot m_x + \frac{3y^2}{\|\hat{\mathbf{r}}\|^2}\cdot m_y + \frac{3yz}{\|\hat{\mathbf{r}}\|^2}\cdot m_z \\ \frac{3xz}{\|\hat{\mathbf{r}}\|^2}\cdot m_x + \frac{3yz}{\|\hat{\mathbf{r}}\|^2}\cdot m_y + \frac{3z^2}{\|\hat{\mathbf{r}}\|^2}\cdot m_z \end{bmatrix} - \begin{bmatrix} m_x \\ m_y \\ m_z \end{bmatrix}$$

$$= \begin{bmatrix} \left(\frac{3x^2}{\|\hat{\mathbf{r}}\|^2} - 1\right)\cdot m_x + \frac{3xy}{\|\hat{\mathbf{r}}\|^2}\cdot m_y + \frac{3xz}{\|\hat{\mathbf{r}}\|^2}\cdot m_z \\ \frac{3xy}{\|\hat{\mathbf{r}}\|^2}\cdot m_x + \left(\frac{3y^2}{\|\hat{\mathbf{r}}\|^2} - 1\right)\cdot m_y + \frac{3yz}{\|\hat{\mathbf{r}}\|^2}\cdot m_z \\ \frac{3xz}{\|\hat{\mathbf{r}}\|^2}\cdot m_x + \frac{3yz}{\|\hat{\mathbf{r}}\|^2}\cdot m_y + \left(\frac{3z^2}{\|\hat{\mathbf{r}}\|^2} - 1\right)\cdot m_z \end{bmatrix} \tag{5.4}$$

$$= \underbrace{\left(3\left(\frac{\hat{\mathbf{r}}}{\|\hat{\mathbf{r}}\|}\right)\left(\frac{\hat{\mathbf{r}}}{\|\hat{\mathbf{r}}\|}\right)^T - I_3\right)}_{K}\mathbf{m}$$

$$= K\mathbf{m}$$

where I_3 is the (3×3)-identity matrix and:

$$K(\mathbf{r}) = \left(3\left(\frac{\hat{\mathbf{r}}}{\|\hat{\mathbf{r}}\|}\right)\left(\frac{\hat{\mathbf{r}}}{\|\hat{\mathbf{r}}\|}\right)^T - I_3\right) \tag{5.5}$$

We plug in the new expression for $\mathbf{B}_{\mu_i}$, given by equation (5.4), in the previously formulated inverse problem, see equation (5.1). Note that because $K(\mathbf{r})$ and $\hat{\mathbf{r}} = \mathbf{r} - \mathbf{d}$, with $\mathbf{r}$ and $\mathbf{d}$ fixed, we are left with the following problem to solve for $\mathbf{B}_0$ and $\mathbf{m}$.

$$\mathbf{B}_0^c + K\mathbf{m} = \mathbf{B}(\mathbf{r}) \tag{5.6}$$

We are now closer to finding a formulation of the inverse problem that is easier to solve. Because the problem is linear in $\mathbf{m}$, we formulate the problem as the linear equation which we know how to solve using linear algebra. So suppose

$$A\mathbf{x} = \mathbf{b} \tag{5.7}$$

where A is an $(m\times n)$-matrix, $\mathbf{b}$ is a $(n\times 1)$-vector with $m, n \in \mathbb{R}^3$ and $\mathbf{x}$ is the column vector of solutions..

We rewrite equation 5.6 to the linear system given by equation 5.7, by multiplying $\mathbf{B}_0^c$ in equation (5.5) with the (3×3)-identity matrix I_3.

$$I_3 \cdot \mathbf{B}_0^c + K\mathbf{m} = \mathbf{B}(\mathbf{r}_j) \tag{5.8}$$

This is equivalent to the following problem:

$$\underbrace{[I_3 \quad K]}_{A}\mathbf{x} = \underbrace{\mathbf{B}(\mathbf{r}_j)}_{\mathbf{b}}, \qquad \text{where } \mathbf{x} = \begin{bmatrix} \mathbf{B}_0^c \\ \mathbf{m}^c \end{bmatrix} = \begin{bmatrix} B_{0_x}^c \\ B_{0_y}^c \\ B_{0_z}^c \\ m_x^c \\ m_y^c \\ m_z^c \end{bmatrix} \tag{5.9}$$

where A is an $(3M \times 3 + 3N)$-matrix, $\mathbf{b}$ is a $(3M \times 1)$-vector. In this case, $M = 1$ and $N = 1$ because we do one measurement and consider one dipole. $\mathbf{x}$ is the column vector of solutions containing the unknown magnetic moment $\mathbf{m}$ and the magnetic background field $\mathbf{B}_0^c$. We see that equation (5.9) is in the form of a linear equation as shown in equation (5.7). If we can find the solution $\mathbf{x}$, we will have found the values for the magnetic background field $\mathbf{B}_0^c$.

The linear formulation of our inverse problem that we need to solve for $\mathbf{x}$ becomes:

$$[I_3 \quad K]\,\mathbf{x} = \mathbf{B}(\mathbf{r}_j) \tag{5.10}$$

We have to keep in mind that this only applies to a problem where we want to measure the magnetic background field with one dipole, and one measurement.

5.3 Solving the inverse problem: the method of least squares

In the previous section we formulated the inverse problem our model will solve. As the system given in equation (5.10) is linear, we formulated the problem as a linear equation (for one measurement and one dipole). And a problem of this form, we know how to solve. It could be done with Gauss elimination, but as the system will grow for more than one measurement and more than one dipole, we use the method of least squares to solve the inverse problem.

The method of least squares. *Suppose A is an $(m \times n)$-matrix, $\mathbf{b}$ is an $(m \times 1)$-vector and $\mathbf{x}$ is an $(n \times 1)$-column vector. Given a over determined system of linear equations:*

$$A\mathbf{x} = \mathbf{b}$$

The solution for $\mathbf{x}$ is given by the well known solution:

$$\hat{\mathbf{x}} = (A^T A)^{-1} A^T \mathbf{b} \tag{5.11}$$

We use this solution for $\mathbf{x}$ to solve the inverse problem given by

$$[I_3 \quad K]\,\mathbf{x} = \mathbf{B} \tag{5.12}$$

We set $A = [I_3 \quad K]$.

5.4 The model for M measurements and N dipoles

We have formulated the forward and inverse problems to develop our model to find the magnetic background field $\mathbf{B}_0$. However all earlier formulation only apply to problems where we do one measurement with one dipole. Figure 5.2 shows what happens to the magnetic field when more than one dipole is placed inside the field.

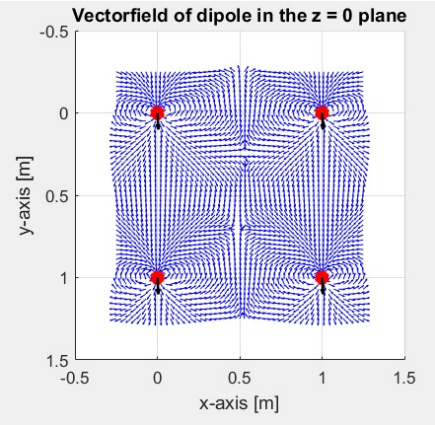

Figure 5.2: The influence on the magnetic field when more dipoles are placed

In this section we extend the model for determining the magnetic background field for M measurements and N dipoles.

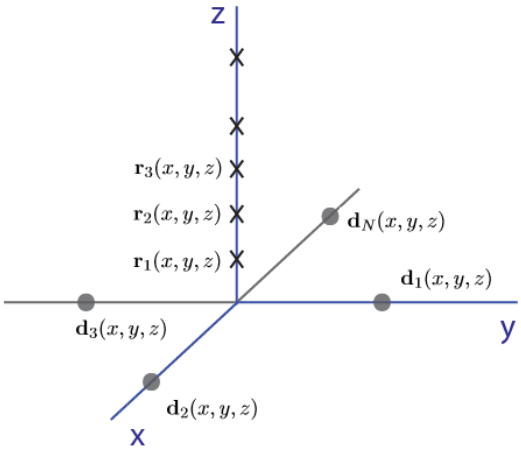

Figure 5.3: Extending the model to M measurements and N dipoles

5.4.1 Formulation for $M = 2$ measurement and $N = 1$ dipole

An important note is that, in order for the linear system, given by equation 5.12, to be determined, one measurements for one dipole is not enough. We need at least two measurements. The explanation for this is given at the end of the next section. For $M = 2$ and $N = 1$ the total magnetic field at locations $\mathbf{r}_1$ and $\mathbf{r}_2$ is given by

$$\mathbf{B}(\mathbf{r}_1, \mathbf{r}_2) = \begin{bmatrix} \mathbf{B}(\mathbf{r}_1) \\ \mathbf{B}(\mathbf{r}_2) \end{bmatrix} = \mathbf{B}_0^c + K\mathbf{m} \tag{5.13}$$

Because $\mathbf{B}$ is now a (6×1)-vector, we must change the dimensions of $\mathbf{B}_0^c$ too. This remains to be the magnetic background field, but we define simply repeat the x, y and z-components.

$$\mathbf{B}_0^c(\mathbf{r}_1, \mathbf{r}_2) = \begin{bmatrix} \mathbf{B}_0^c \\ \mathbf{B}_0^c \end{bmatrix} \tag{5.14}$$

Also because we have one dipole, measured from two different locations we obtain a K as followed:

$$K = \begin{bmatrix} K(\mathbf{r}_1) \\ K(\mathbf{r}_2) \end{bmatrix}$$

Where $K(\mathbf{r}_1)$ is the matrix K with $\hat{\mathbf{r}} = \mathbf{r}_1 - \mathbf{d}$ and $K(\mathbf{r}_2)$ is the matrix K with $\hat{\mathbf{r}} = \mathbf{r}_2 - \mathbf{d}$. After rewriting equation (5.13) to a linear problem $A\mathbf{x} = \mathbf{b}$, the solution $\mathbf{x}$, will only contain $\mathbf{B}_0^c$ once, so we still have:

$$\mathbf{x} = \begin{bmatrix} \mathbf{B}_0^c \\ \mathbf{m}^c \end{bmatrix} = \begin{bmatrix} {B_0}_x^c \\ {B_0}_y^c \\ {B_0}_z^c \\ m_x^c \\ m_y^c \\ m_z^c \end{bmatrix}$$

We assume $\mathbf{B}_0^c$ is the same for both $\mathbf{r}_1$ and $\mathbf{r}_2$ because earth's magnetic field is locally uniform.

When $M = 2$ and $N = 1$, we can solve the problem analytically. But the problem becomes harder to solve when $M, N > 1$ because the dimensions of $\mathbf{B}(r_j), \mathbf{B}_0^c$ and $\mathbf{B}_i = K\mathbf{m}$ continue to grow. The dimensions can be in the table found below

	Description	Dimension
$\mathbf{B}(\mathbf{r}_1, \mathbf{r}_2)$	The measured magnetic field, measured by the sensors. The sensors measure the total $\mathbf{B}$-field in the x, y and z-direction at locations $\mathbf{r}_1$ and $\mathbf{r}_2$	6×1
$\mathbf{B}_0^c$	The computed magnetic background field. A vector describing the magnetic background field in the x, y and z-directions	3×1
K	A matrix used to linearize the problem	3×3
A	A matrix used to linearize the problem	2×6
$\hat{\mathbf{x}}$	The solution vector containing $\mathbf{B}_0^c$ and $\mathbf{m}$	6×1

We will see that for $M, N > 1$, the dimensions indeed grow and we will look at in what manner they will do so in the next section. This helps us determine how to formulate the problem for M measurements and N dipoles and what restricts our model.

5.4.2 Formulation for M measurements and N dipoles

Going back to what we know, we have

$$\mathbf{B}(\mathbf{r}_j) = \mathbf{B}_0 + \mathbf{B}_{\mu_1} + \mathbf{B}_{\mu_2} + ... + \mathbf{B}_{\mu_N}$$

In this section we see what this expression means and what it looks like for M measurements and N dipoles.

Suppose we have M measurements: $\mathbf{B}(\mathbf{r}_1), \mathbf{B}(\mathbf{r}_2), ..., \mathbf{B}(\mathbf{r}_M)$. We define the measured magnetic field $\mathbf{B}(\mathbf{r}_j)$ as followed:

$$\mathbf{B}(\mathbf{r}_j) = \begin{bmatrix} \mathbf{B}(\mathbf{r}_1) \\ \mathbf{B}(\mathbf{r}_2) \\ \vdots \\ \mathbf{B}(\mathbf{r}_M) \end{bmatrix} \tag{5.15}$$

Each $\mathbf{B}(\mathbf{r}_j)$ is a (3×1)-vector at some location $\mathbf{r}_j$ for $j \in \{1, 2, ..., M\}$. So $\mathbf{B}(\mathbf{r}_j)$ for M measurements consists of each x, y and z-component of each measured field at locations $\mathbf{r}_1, \mathbf{r}_2, ..., \mathbf{r}_M$. Now suppose we have N dipoles on locations $\mathbf{d}_1, \mathbf{d}_2, \mathbf{d}_3, ..., \mathbf{d}_N$. Then the magnetic field of the dipole μ_i with location $\mathbf{d}_i$, for $i \in \{1, 2, ..., N\}$ and sensor location $\mathbf{r}_j$ is given by

$$\mathbf{B}_{\mu_i} = \frac{\mu_0}{4\pi} \left[\frac{(\mathbf{m}_i \cdot \hat{\mathbf{r}}_{ij})\hat{\mathbf{r}}_{ij}}{\|\hat{\mathbf{r}}_{ij}\|^5} - \frac{\mathbf{m}_i}{\|\hat{\mathbf{r}}_{ij}\|^3} \right] \tag{5.16}$$

So now we can rewrite equation (5.4.2), and we can conclude that it is equivalent to the equation (5.17), where each component is another (3×1)-vector.

$$\begin{bmatrix} \mathbf{B}(\mathbf{r}_1) \\ \mathbf{B}(\mathbf{r}_2) \\ \mathbf{B}(\mathbf{r}_3) \\ \vdots \\ \mathbf{B}(\mathbf{r}_M) \end{bmatrix} = \begin{bmatrix} \mathbf{B}_0 \\ \mathbf{B}_0 \\ \mathbf{B}_0 \\ \vdots \\ \mathbf{B}_0 \end{bmatrix} + \begin{bmatrix} \mathbf{B}_{\mu_1}(\mathbf{r}_1) + \mathbf{B}_{\mu_2}(\mathbf{r}_1) + \mathbf{B}_{\mu_3}(\mathbf{r}_1) + ... + \mathbf{B}_{\mu_N}(\mathbf{r}_1) \\ \mathbf{B}_{\mu_1}(\mathbf{r}_2) + \mathbf{B}_{\mu_2}(\mathbf{r}_2) + \mathbf{B}_{\mu_3}(\mathbf{r}_2) + ... + \mathbf{B}_{\mu_N}(\mathbf{r}_2) \\ \mathbf{B}_{\mu_1}(\mathbf{r}_3) + \mathbf{B}_{\mu_2}(\mathbf{r}_3) + \mathbf{B}_{\mu_3}(\mathbf{r}_3) + ... + \mathbf{B}_{\mu_N}(\mathbf{r}_3) \\ \vdots \\ \mathbf{B}_{\mu_1}(\mathbf{r}_M) + \mathbf{B}_{\mu_2}(\mathbf{r}_M) + \mathbf{B}_{\mu_3}(\mathbf{r}_M) + ... + \mathbf{B}_N(\mathbf{r}_M) \end{bmatrix} \tag{5.17}$$

To find the magnetic background field $\mathbf{B}_0$ from equation (5.17), we introduce another matrix K' and another matrix A' similar to the matrices in equation (5.5) and equation (5.9), but extended to different dimensions. Afterwards, we solve the inverse problem with the method of least squares.

$$\underbrace{\begin{bmatrix} \mathbf{B}(\mathbf{r}_1) \\ \mathbf{B}(\mathbf{r}_2) \\ \mathbf{B}(\mathbf{r}_3) \\ \vdots \\ \mathbf{B}(\mathbf{r}_M) \end{bmatrix}}_{\mathbf{B}(\mathbf{r})'} = \underbrace{\begin{bmatrix} \mathbf{B}_0 \\ \mathbf{B}_0 \\ \mathbf{B}_0 \\ \vdots \\ \mathbf{B}_0 \end{bmatrix}}_{\mathbf{B}_0'} + \underbrace{\begin{bmatrix} \mathbf{B}_{\mu_1}(\mathbf{r}_1) + \mathbf{B}_{\mu_2}(\mathbf{r}_1) + \mathbf{B}_{\mu_3}(\mathbf{r}_1) + ... + \mathbf{B}_{\mu_N}(\mathbf{r}_1) \\ \mathbf{B}_{\mu_1}(\mathbf{r}_2) + \mathbf{B}_{\mu_2}(\mathbf{r}_2) + \mathbf{B}_{\mu_3}(\mathbf{r}_2) + ... + \mathbf{B}_{\mu_N}(\mathbf{r}_2) \\ \mathbf{B}_{\mu_1}(\mathbf{r}_3) + \mathbf{B}_{\mu_2}(\mathbf{r}_3) + \mathbf{B}_{\mu_3}(\mathbf{r}_3) + ... + \mathbf{B}_{\mu_N}(\mathbf{r}_3) \\ \vdots \\ \mathbf{B}_{\mu_1}(\mathbf{r}_M) + \mathbf{B}_{\mu_2}(\mathbf{r}_M) + \mathbf{B}_{\mu_3}(\mathbf{r}_M) + ... + \mathbf{B}_N(\mathbf{r}_M) \end{bmatrix}}_{\mathbf{B}_{\mu_i}(\mathbf{r}_j)'} \tag{5.18}$$

We know from section 5.2 that we can rewrite

$$\mathbf{B}(\mathbf{r})' = \mathbf{B}_0' + \mathbf{B}_{\mu_i}(\mathbf{r}_j)'$$

as a linear inverse problem with the possibility to be solved with the method of least squares. We use a matrix K' and A' for M measurements and N dipoles. Recall

$$K(\mathbf{r}) = \left(3 \left(\frac{\hat{\mathbf{r}}}{\|\hat{\mathbf{r}}\|} \right) \left(\frac{\hat{\mathbf{r}}}{\|\hat{\mathbf{r}}\|} \right)^T - I_3 \right) \quad \text{with} \quad A = [I_3 \quad K]$$

to solve $[I_3 \quad K]\mathbf{x} = \mathbf{B}(\mathbf{r}_j)$. By the method of least squares, we find $\mathbf{x}$ in:

$$A\mathbf{x} = [I_3 \quad K] \begin{bmatrix} \mathbf{B}_{0x}^c \\ \mathbf{B}_{0y}^c \\ \mathbf{B}_{0z}^c \\ \mathbf{m}_x \\ \mathbf{m}_y \\ \mathbf{m}_z \end{bmatrix} = \mathbf{B}_m \tag{5.19}$$

The vector $\hat{\mathbf{r}}$ represents the difference between the j^{th} measurement location and the i^{th} dipole. Therefore if we have M measurements and one dipole at location $\mathbf{d}_1$, so $N = 1$, then we would get:

$$\hat{\mathbf{r}} = \mathbf{r}_j - \mathbf{d}_i = \begin{bmatrix} \mathbf{r}_1 - \mathbf{d}_1 \\ \mathbf{r}_2 - \mathbf{d}_1 \\ \mathbf{r}_3 - \mathbf{d}_1 \\ \vdots \\ \mathbf{r}_M - \mathbf{d}_1 \end{bmatrix} \tag{5.20}$$

Note that $j = 1, 2, ..., M$.

Now for one measurement at location $\mathbf{r}_1$, so $M = 1$ and N dipoles with magnetic moments $\mathbf{m}_1, \mathbf{m}_2, ..., \mathbf{m}_N$, we find that the magnetic field of N dipoles, all observed from location $\mathbf{r}_1$, is given by

$$\begin{aligned} \mathbf{B}_\mu &= \mathbf{B}_{\mu_1} + \mathbf{B}_{\mu_2} + \mathbf{B}_{\mu_3} + ... + \mathbf{B}_{\mu_N} \\ &= K_{1,1}\mathbf{m}_1 + K_{1,2}\mathbf{m}_2 + K_{1,3}\mathbf{m}_3 + ... + K_{N,1}\mathbf{m}_N \\ &= [K_{1,1} \quad K_{1,2} \quad K_{1,3} \quad .... \quad K_{1,N}] \begin{bmatrix} \mathbf{m}_1 \\ \mathbf{m}_2 \\ \mathbf{m}_3 \\ \vdots \\ \mathbf{m}_N \end{bmatrix} \end{aligned} \tag{5.21}$$

Here, $K_{1,i}$ is the matrix K with $\hat{\mathbf{r}} = \mathbf{r}_1 - \mathbf{d}_i$ for $i = 1, 2, ..., N$.

If we combine the expression obtained in (5.21) with the formulation of the non linear inverse problem, we find that for M measurements and N dipoles.

$$\mathbf{B}_0^c + \mathbf{B}_\Omega^c = \mathbf{B}(\mathbf{r}_j)$$

is equivalent to the following:

$$\underbrace{\begin{bmatrix} I_3 & \mathbf{B}_0^c \\ I_3 & \mathbf{B}_0^c \\ I_3 & \mathbf{B}_0^c \\ \vdots & \vdots \\ I_3 & \mathbf{B}_{0c} \end{bmatrix}}_{[I_3 \quad \mathbf{B}_0^{c\prime}]} + \underbrace{\begin{bmatrix} K_{1,1} & K_{1,2} & K_{1,3} & .... & K_{1,N} \\ K_{2,1} & K_{2,2} & K_{2,3} & .... & K_{2,N} \\ K_{3,1} & K_{3,2} & K_{3,3} & .... & K_{3,N} \\ \vdots & \vdots & \vdots & \vdots & \vdots \\ K_{M,1} & K_{M,2} & K_{M,3} & .... & K_{M,N} \end{bmatrix}}_{K'} \underbrace{\begin{bmatrix} \mathbf{m}_1 \\ \mathbf{m}_2 \\ \mathbf{m}_3 \\ \vdots \\ \mathbf{m}_N \end{bmatrix}}_{\mathbf{m}'} = \underbrace{\begin{bmatrix} \mathbf{B}_{m,1} \\ \mathbf{B}_{m,2} \\ \mathbf{B}_{m,3} \\ \vdots \\ \mathbf{B}_{m,M} \end{bmatrix}}_{\mathbf{B}(\mathbf{r}_j)'} \tag{5.22}$$

$$[I_3 \quad \mathbf{B}_0^c]' + K'\mathbf{m}' = \mathbf{B}(\mathbf{r}_j)' \tag{5.23}$$

Where $\mathbf{B}_0^c$ is the magnetic background field we are looking for, $K_{j,i}$ is the (3×3)-matrix K we need to solve the inverse problem for the j^{th} measurement and i^{th} dipole, with $i = 1, 2, 3..., M$ and $j = 1, 2, 3, ..., N$. The magnetic moment for each dipole at location $\mathbf{d}_i$ is given by $\mathbf{m}_i$ and each measured magnetic field at sensor location $\mathbf{r}_j$ is given by $\mathbf{B}(\mathbf{r}_j)$.

In the same way as for one measurement and one dipole, we can define the $(3M \times (3 + 3N)$-matrix A' and the solution $\hat{\mathbf{x}}'$ found with the method of least squares:

$$A' = \begin{bmatrix} I_3 & K_{1,1} & K_{1,2} & K_{1,3} & .... & K_{1,N} \\ I_3 & K_{2,1} & K_{2,2} & K_{2,3} & .... & K_{2,N} \\ I_3 & K_{3,1} & K_{3,2} & K_{3,3} & .... & K_{3,N} \\ \vdots & \vdots & \vdots & \vdots & \vdots & \vdots \\ I_3 & K_{M,1} & K_{M,2} & K_{M,3} & .... & K_{M,N} \end{bmatrix} \quad \text{and} \quad \hat{\mathbf{x}}' = \begin{bmatrix} \mathbf{B}_0^c \\ \mathbf{m}' \end{bmatrix} = \begin{bmatrix} \mathbf{B}_0^c \\ \mathbf{m}_1 \\ \mathbf{m}_2 \\ \mathbf{m}_3 \\ \vdots \\ \mathbf{m}_N \end{bmatrix} \tag{5.24}$$

Before using (5.3) to determine $\mathbf{B}_0$ we should look at the dimensions first.

	Description	Dimension
$\mathbf{B}(\mathbf{r}_j)$	The measured magnetic field, measured by one of the M sensors	$3M \times 1$
$\mathbf{B}_0^{c\prime}$	The computed magnetic background field for M measurements. This means its repeats $\mathbf{B}_0^c$ M times	$3N \times 1$
K'	A matrix used to linearize the problem	3×3
A'	A matrix used to linearize the problem	$3M \times (3N + 3)$
$\mathbf{B}_\mu$	The sum of all calculated magnetic fields of N dipoles	$3M \times 1$
$\hat{\mathbf{x}}'$	The solution vector containing $\mathbf{B}_{0c}$ and $\mathbf{m}$	$(3N + 3) \times 1$

Note that when solving the inverse problem, the amount of unknown variables should not exceed the amount of known variables. In this case we have M known measurements of the total $\mathbf{B}$-field, this means we have 3 known components for each unknown $\mathbf{B}$-field, resulting in $3M$ known variables. We have N unknown $\mathbf{B}$-fields of each dipole, resulting in $3N$ unknown variables. Lastly, we have 3 unknown components of the magnetic background field $\mathbf{B}_0$ we want to determine. In order for the unknown not to exceed the known, we should choose the amount of dipoles and measurements in any experiment such tat

$$3M > 3 + 3N$$

In the next chapters, when referring to the linear system we want to solve

$$A\mathbf{x} = \mathbf{b}$$

we mean the linear system given by equation (5.19) where the solution $\mathbf{x}$ contains the computed magnetic background field $\mathbf{B}_0^c$ and the determined magnetic moments $\mathbf{m}$.

5.5 An acceptable result

Before testing our model on some data set for M measurements and N locations, we have to define what makes the result for $\mathbf{B}_{0c}$ acceptable. If we've found an acceptable solution, we can try to improve it if needed.

There are two ways in which we can obtain some information on an acceptable solution. We can construct images to compare the result $\mathbf{B}_{0c}$ to the true background field $\mathbf{B}_0$, or we can look at the approximation errors: the absolute and relative error.

5.5.1 The absolute error

Given some value v and its approximation v', we define the absolute error by

$$\epsilon = \|v - v'\| \tag{5.25}$$

So when looking at the absolute error, we're simply considering the magnitude of the difference between values v and v'. This can give us some insight on how much our calculated differs from the true magnetic background field.

5.5.2 The relative error

Given some value v and its approximation v', we define the absolute error by

$$\tau = \frac{\|v - v'\|}{\|v\|} \tag{5.26}$$

Multiplying the relative error by a 100% gives us the percentage error and this gives us some insight on how much percent the approximation v' differs from the exact value v.

We can expand these definitions to vectors in $\mathbb{R}^n$, which we do for our research as well. As a rule of thumb, we use that if the relative error is no greater then 0.10 or equivalently, if the approximation v' differs no more than 10% from the exact value v, we have an acceptable approximation.

We use this rule of thumb to determine whether our calculated $\mathbf{B}_0^c$ is an acceptable approximation for the true $\mathbf{B}_0$.

Chapter 6

Noise and numerical instability

For this research, we used the model on real data. But in reality, the sensors, especially cheap ones, are not fully trustworthy. There is always some noise in the measurements because the sensors are not fully consistent. This means that we have to adjust our model keeping in mind that we will have to correct some of the noise we detect with the sensors. We correct the errors because of the noise with the use of regularization, something that is explained in chapter 7. In this chapter we adjust the model by including a certain amount of noise.

6.1 Noise model: Gaussian Noise

Every data point we acquire with the sensors includes a certain amount of noise. Consider $\mathbf{e}$ to be the noise vector we measure in addition to the true measured field. Each δ_i for $i = 1, .., M$ is the noise for every i^{th} measurement. We have

$$\mathbf{e} = \begin{bmatrix} \delta_1 \\ \delta_2 \\ \vdots \\ \delta_M \end{bmatrix} \tag{6.1}$$

To avoid any confusion, we will call $\mathbf{B}_e$ the exact measured magnetic field without noise. The measured field at location $\mathbf{r}$ that includes noise is then given by

$$\mathbf{B}(\mathbf{r}) = \mathbf{B}_e(\mathbf{r}) + \mathbf{e} \tag{6.2}$$

To model each entry δ_i of $\mathbf{e}$ we use the Gaussian Noise model. Gaussian noise arises in images due to sensor noise caused by natural sources such as thermal vibrations of atoms in conductors, shot noise or electronic circuit noise [9].

For each measurement vector without noise $\mathbf{B}_e$, we have that

$$\delta \sim N(\mu = 0, \sigma^2 I_3) \tag{6.3}$$

where the probability density function of a Gaussian random variable z is given by

$$p_G(z) = \frac{1}{\sqrt{2\pi}\sigma} e^{\frac{-(z-\mu)^2}{2\sigma^2}} \tag{6.4}$$

Here z represents the grey level, μ the mean value and σ the standard deviation.

To know exactly what $\mathbf{e}$ is, we need σ to model each entry δ_i. It is stated in [1] that when we measure the magnetic field inside a steel object using a sensor, experience finds that the measurement can deviate no more than 300 nanotesla for each sensor location $\mathbf{r}$, so

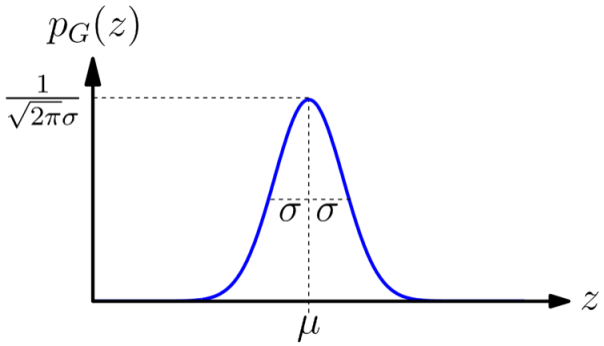

Figure 6.1: Gaussian probability density function $P_G(z)$ [9]

$$\|\mathbf{B}_e(\mathbf{r}) - \mathbf{B}(\mathbf{r})\| \leq 300 \text{ nT} \tag{6.5}$$

This results in a reasonable value for σ given by

$$3\sigma = \frac{1}{3}\sqrt{3} \cdot 300 \cdot 10^{-9} \quad \text{and} \quad \mu \pm 3\sigma = 99$$

This is equivalent to

$$\sigma = \frac{1}{9}\sqrt{3} \cdot 100 \cdot 10^{-9} \tag{6.6}$$

6.2 Revised model including noise

We now have a revised model that includes the noise real sensors would measure. The measured magnetic field is the sum of the exact, sole measured magnetic field $\mathbf{B}_e$ and the noise $\mathbf{e}$

$$\mathbf{B} = \mathbf{B}_e + \mathbf{e}$$

Applying this to our inverse model, we find that the inverse problem can be formulated by

$$A\mathbf{x} = \mathbf{B}_e + \mathbf{e} \tag{6.7}$$

Where $\mathbf{x}$ is the solution containing the computed magnetic background field $\mathbf{B}_0$ and A is still the matrix containing the (3×3)-identity matrices and (3×3)-matrices K.

Depending on the physical properties of A, there might not always be an exact solution $\hat{\mathbf{x}}$ to the problem (6.7). The method of least squares uses *singular value decomposition* to find a solution near $\hat{\mathbf{x}}$. In the next chapter we will see why some linear systems of the form $A\mathbf{x} = \mathbf{b}$ are unstable.

6.3 Singular value decomposition

Consider the inverse problem without noise, a linear system of the form

$$A\mathbf{x} = \mathbf{b} \tag{6.8}$$

If A were to be a square matrix, it would be easy to find a solution. But that is not necessarily the case for A, as the dimensions of A depend on the amount of measurements M and the number of dipoles N. To such matrices, we apply singular value decomposition.

Theorem 6.3.1. *Singular Value Decomposition (SVD). Let $A \in \mathbb{R}^{m\times n}$ be a matrix of rank r. Then there exist orthogonal matrices $U \in \mathbb{R}^{m\times m}$ and $R \in \mathbb{C}^{n\times n}$ such that*

$$A = U\Sigma V^T, \quad \Sigma = \begin{bmatrix} \Sigma_1 & 0 \\ 0 & 0 \end{bmatrix} \tag{6.9}$$

where $\Sigma \in \mathbb{R}^{m\times n}, \Sigma_1 = diag(\sigma_1, \sigma_2, ..., \sigma_r)$ with σ_n the singular values of A, and

$$\sigma_1 \geq \sigma_2 \geq ... \geq \sigma_r > 0$$

The singular values of A are defined by

$$A\mathbf{v}_n = \sigma_n \mathbf{u}_n$$

with $\mathbf{u}_n$ and $\mathbf{v}_n$ are the columns of the matrices U and V respectively.

If there is no exact solution to the system in expression (6.8), we can approximate its solution $\mathbf{x}_e$ using the *pseudo-inverse* of A given by $A^\dagger$ and the solution $\mathbf{x}^\dagger$. We have

$$\mathbf{x}^\dagger = A^\dagger \mathbf{b} \tag{6.10}$$

And the pseudo-inverse of A can be written as

$$A^\dagger = (U\Sigma V^T)^\dagger = V\Sigma^\dagger U^T \tag{6.11}$$

This results in an expression for the best-approximate solution $\mathbf{x}^\dagger$ of $\mathbf{x}_e$, which is the exact solution of the linear system $A\mathbf{x} = \mathbf{b}$. See the derivation of $\mathbf{x}^\dagger$ below. We have

$$\mathbf{x}^\dagger = A^\dagger \mathbf{b} = (U\Sigma V^T)^\dagger \mathbf{b} = V\Sigma^\dagger U^T \mathbf{b} \tag{6.12}$$

So we found

$$\mathbf{x}^\dagger = V\Sigma^\dagger U^T \mathbf{b} \tag{6.13}$$

Recall $V = [\mathbf{v}_1 \quad \mathbf{v}_2 \quad ... \quad \mathbf{v}_n], \quad U = [\mathbf{u}_1 \quad \mathbf{u}_2 \quad ... \quad \mathbf{u}_m]$ and

$$\Sigma = \begin{bmatrix} \Sigma_1 & 0 \\ 0 & 0 \end{bmatrix} \quad \text{with} \quad \Sigma_1 = \left[\begin{array}{cccc|c} \sigma_1 & 0 & \cdots & \cdots & \cdots \\ 0 & \sigma_2 & 0 & \cdots & \cdots \\ \vdots & 0 & \ddots & 0 & 0 \\ \vdots & \vdots & 0 & \sigma_r & 0 \\ \hline \vdots & \vdots & \vdots & 0 & 0 \end{array}\right] \quad \text{for } r \text{ eigenvalues}$$

The pseudo-inverse of A is defined by $A^\dagger = (A^T A)^{-1} A^T$, [1]. We can also write

$$\Sigma^\dagger = \begin{bmatrix} \Sigma_1^{-1} & 0 \\ 0 & 0 \end{bmatrix} \quad \text{and} \quad U^T\mathbf{b} = \begin{bmatrix} \mathbf{u}_1^T\mathbf{b} \\ \mathbf{u}_2^T\mathbf{b} \\ \vdots \\ \mathbf{u}_m^T\mathbf{b} \end{bmatrix} \tag{6.14}$$

We substitute the expressions in (6.14) in equation (6.11). We find for the solution $\mathbf{x}^\dagger$:

$$\begin{aligned} \mathbf{x}^\dagger &= V\Sigma^\dagger U^T \mathbf{b} \\ &= V \begin{bmatrix} \frac{1}{\sigma_1} & \mathbf{u}^T\mathbf{b} \\ \frac{1}{\sigma_2} & \mathbf{u}^T\mathbf{b} \\ \vdots & \vdots \\ \frac{1}{\sigma_r} & \mathbf{u}^T\mathbf{b} \end{bmatrix} = \sum_{i=1}^{r} \left(\frac{\mathbf{u}_i^T\mathbf{b}}{\sigma_i}\right)\mathbf{v}_i \end{aligned}$$

The method of least squares uses this solution

$$\mathbf{x}^\dagger = \sum_{i=1}^{r} \left(\frac{\mathbf{u}_i^T \mathbf{b}}{\sigma_i} \right) \mathbf{v}_i \tag{6.15}$$

as it will look for the "nearest" solution to $\mathbf{x}_e$. Therefore $\hat{\mathbf{x}} = A^\dagger \mathbf{b}$ is exactly the least squares solution of the linear system $A\mathbf{x} = \mathbf{b}$. This concludes that we can easily find a solution that approximates $\mathbf{x}_e$ of $A\mathbf{x} = \mathbf{b}$ if we know the singular value decomposition of A.

6.4 Numerical instability

The solution we acquired in equation (6.15) will not always provide the best solution. We also ignored the possibility of noise in computing a solution via the singular value decomposition. Suppose we want to solve the system $A\mathbf{x} = \mathbf{b}$, where $\mathbf{b}$ is subject to noise:

$$\mathbf{b} = \mathbf{b}_e + \mathbf{e}$$

We consider $\mathbf{x}_e$ to be the exact solution of $A\mathbf{x} = \mathbf{b}_e$ where there is no noise present.

The *condition number* $\kappa(A)$ of a matrix A gives us some insight on whether a solution is reliable. The condition number measures how much the output of a function can change for a small change in the input, meaning we can measure the sensitivity of a function. The condition number of a problem depends on the physics of the matrix A that is to be inverted in the problem. A problem with a low condition number is considered *well-conditioned*, and a problem with a high condition number is said to be *ill-conditioned*.

The condition number of a problem $A\mathbf{x} = \mathbf{b}$ is defined as

$$\kappa := \frac{\sigma_{max}}{\sigma_{min}} \tag{6.16}$$

where $\sigma_{max} = \sigma_1 \geq \sigma_2 \geq ... \geq \sigma_r = \sigma_{min} > 0$ are the singular values of A.

We see that if that for singular values $\sigma_{min} \leq \sigma_i << 1$, the condition number $\kappa(A)$ becomes very large. The consequence of a large condition number can be explained with the following theorem:

Theorem 6.4.1. *Suppose that* $A \in^m$ *and* $\mathbf{b}, \mathbf{e} \in \mathbb{R}^m$ *nonzero vectors. Assume that* $A\mathbf{x}_e = \mathbf{b}$ *and* $A\mathbf{x} = \mathbf{b} + \mathbf{e}$ *hold. Then*

$$\frac{\|\mathbf{x} - \mathbf{x}_e\|}{\|\mathbf{x}_e\|} \leq \kappa(A) \frac{\|\mathbf{e}\|}{\|\mathbf{b}\|}$$

This lemma implies that a matrix with a large condition number, hence and ill-conditioned matrix A, computes solutions that are very sensitive (small) perturbations $\mathbf{e}$. When solving the system $A\mathbf{x} = \mathbf{b}_e + \mathbf{e}$ using the pseudo inverse and singular value decomposition, we find:

$$\mathbf{x}^\dagger := A^\dagger(\mathbf{b}_e + \mathbf{e}) = \sum_{i=1}^{r} \frac{\mathbf{u}_i^T \mathbf{b}_e}{\sigma_i} \mathbf{v}_i + \sum_{i=1}^{r} \frac{\mathbf{u}_i^T \mathbf{e}}{\sigma_i} \mathbf{v}_i \tag{6.17}$$

A short derivation of equation (6.17) can be found in chapter eight.

When we have singular values $\sigma_{min} \leq \sigma_i << 1$, the noisy term in equation (6.17) becomes very large and therefore having great influence on the solution $\mathbf{x}^\dagger$. This causes a great difference between the exact solution $\mathbf{x}_e$ and $\mathbf{x}^\dagger$.

In this research, we use the condition number in the same sense that an ill-conditioned problem means that small noise or measurement errors can influence the output greatly, which can be explained

with Theorem 6.4.1. As a rule of thumb, if $\kappa(A) \sim 10^k$, then the solution loses up to k digits in accuracy on top of what would already be lost in numerical methods, in comparison to arithmetical methods. We also say that a problem has a large condition number if it is in the order of $k \geq 6$ [1]. In the next chapter we see that there is a way where we do not have to deal with the smallest singular values.

Chapter 7

Regularization methods

The current situation requires us to solve an inverse problem $A\mathbf{x} = \mathbf{b}$ using the method of least squares, a direct solving method. This method relies on the singular value decomposition of A. Depending on the physics and singular values of A, the solution we obtain via the method of least squares, may not be the most optimal or feasible. In this section we take a look at some other methods, more advance solvers, where we try to make the problem less sensitive to noise by changing the problem, this is called *regularization*.

Regularization is the process where we reduce the influence of noise, by adding more information to the solution $\mathbf{x}$ to produce an augmented set of feasible solutions [1]. In this section, we look at two regularization methods.

Suppose we have the usual linear system to solve

$$A\mathbf{x} = \mathbf{b}$$

And suppose this is a system where $\mathbf{b}$ is subject to noise $\mathbf{e}$ so A is the $m \times n$ forward matrix and we have

$$\mathbf{b} = \mathbf{b}_e + \mathbf{e}$$

The exact solution we are looking for is the solution of $A\mathbf{x} = \mathbf{b}_e$, that is $\mathbf{x}_e$. We obtain this solution by decomposing A as we did in the previous chapter via the singular value decomposition. We decompose A as followed

$$A = U\Sigma V^T, \quad \text{and} \quad \sigma_1 \geq \sigma_2 \geq ... \geq \sigma_r > 0 \quad \text{the singular values of } A.$$

We obtain the following solution:

$$\begin{aligned} \mathbf{x}^\dagger &= A(\mathbf{b}_e + \mathbf{e}) \\ &= A^\dagger \mathbf{b}_e + A^\dagger \mathbf{e} \\ &= \sum_{i=1}^{r} \frac{\mathbf{u}_i^T \mathbf{b}_e}{\sigma_i} \mathbf{v}_i + \sum_{i=1}^{r} \frac{\mathbf{u}_i^T \mathbf{e}}{\sigma_i} \mathbf{v}_i \end{aligned} \tag{7.1}$$

Note that the noisy term $\mathbf{e}$ results in $\mathbf{x}^\dagger$ drifting away from the exact solution $\mathbf{x}_e$. If a matrix A were to be ill-conditioned, then the second summation in (7.1) becomes a large term, influencing the solution. Now we apply regularization to reduce the influence of the second summation, reducing the difference between the solutions $\mathbf{x}^\dagger$ and $\mathbf{x}_e$.

7.1 Truncated singular value decomposition

Suppose we have a matrix A that is ill-conditioned and has both small and large singular values σ_i. The truncated singular value decomposition makes a clear distinction between the two. This method only

takes into account those singular values that have the least influence on $\mathbf{x}^\dagger$. Hence, the singular values for which

$$\sum_{i=1}^{r} \frac{\mathbf{u}_i^T \mathbf{e}}{\sigma_i} \|\mathbf{v}_i\| \approx \sum_{i=1}^{r} \frac{\mathbf{u}_i^T \mathbf{b}_e}{\sigma_i} \|\mathbf{v}_i\|$$

We see that this is the case for $\sigma_i >> 1$, that is the first few singular values $\sigma_1, ..., \sigma_k$ for $k < r$. So for this new solution, we only take into account the first k components of the solution obtained in (7.1). The rest of terms, dominated by the noise, are simply chopped off. How we choose this k depends on the singular values which can be divided two groups singular values. We take into account the large values $\sigma_1, \sigma_2, ...\sigma_k$ and we neglect the small values $\sigma_{k+1}, \sigma_{k+2}, ..., \sigma_r$.

The truncated singular value decomposition changes the matrix A to a matrix A_k using the regularization parameter $k < r = rank(A)$, such that $\kappa(A_k) < \kappa(A)$ for the condition numbers of A and A_k.

For the matrix A we take into account all singular values $_1 > \sigma_2 > ... > \sigma_r$ and define the condition number as:

$$\kappa(A) = \frac{\sigma_{max}}{\sigma_{min}} = \frac{\sigma_1}{\sigma_r}$$

For the matrix A_k we only take into account the larger singular values, so all $\sigma_1 > \sigma_2 > ... > \sigma_k$ for $k < r$. We define the condition number as:

$$\kappa(A_k) = \frac{\sigma_{max}}{\sigma_{min}} = \frac{\sigma_1}{\sigma_k}$$

Because $\sigma_k > \sigma_r$, we find that $\kappa(A_k) < \kappa(A)$ resulting in a better conditioned problem, and therefore more stable than before the regularization.

The solution we obtain is called the truncated singular value decomposition solution $\mathbf{x}_k$ and is given by

$$\mathbf{x}_k = \sum_{i=1}^{k} \frac{\mathbf{u}_i^T \mathbf{b}}{\sigma_i} \mathbf{v}_i \quad \text{for some} \quad k \leq r \tag{7.2}$$

Now we can question what value we should choose for the *regularization parameter* k. Obviously we choose k such that the noise dominant terms are ignored, but what the exact value is, depends on the specific problem that requires solving.

7.2 Conjugate gradient least squares

Another method we can try is the conjugate gradient least squares method. This method computes the least squares solution by iterating k times, expanding the span of solutions. Every iteration comes up with a more accurate solution than the previous iteration. The prediction model for this research uses the TSVD and therefore a more detailed explanation of this method, the CGLS, can be found in [10].

Chapter 8

A twin experiment

In this section we do a twin experiment, meaning we solve a forward problem followed by the inverse problem. The forward problem provides us with a simulated data set and the inverse problem computes the magnetic background field. The result of this experiment answers our question about whether the the system in our model is consistent and whether the solution obtained by our model produces an acceptable result. If we have a consistent model, we are ready to test the model on real data obtained by the Seven Sensors.

For this experiment we choose $M = 4$ measurements and $N = 3$ dipoles. Note that this amount of dipoles meets the requirements for the maximum amount of dipoles (see section 5.4.2).

Suppose all our dipoles have a different magnetic moment, in each a different direction. We arbitrarily choose:

$$\mathbf{m}_1 = \begin{bmatrix} 100 \\ 0 \\ 0 \end{bmatrix}, \quad \mathbf{m}_2 = \begin{bmatrix} 0 \\ 20 \\ 0 \end{bmatrix}, \quad \text{and} \quad \mathbf{m}_3 = \begin{bmatrix} 0 \\ 0 \\ 120 \end{bmatrix}$$

We place our dipoles in the following positions:

$$\mathbf{d}_1 = \begin{bmatrix} -1 \\ 0 \\ 0 \end{bmatrix}, \quad \mathbf{d}_2 = \begin{bmatrix} 0 \\ 0 \\ 0 \end{bmatrix}, \quad \text{and} \quad \mathbf{d}_3 = \begin{bmatrix} 1 \\ 0 \\ 0 \end{bmatrix}$$

The measurements along the z-axis are done in the following sensor locations

$$\mathbf{r}_1 = \begin{bmatrix} 1 \\ 0 \\ 0 \end{bmatrix}, \quad \mathbf{r}_2 = \begin{bmatrix} 2 \\ 0 \\ 0 \end{bmatrix}, \quad \mathbf{r}_3 = \begin{bmatrix} 3 \\ 0 \\ 0 \end{bmatrix}, \quad \text{and} \quad \mathbf{r}_4 = \begin{bmatrix} 4 \\ 0 \\ 0 \end{bmatrix}$$

8.1 Forward simulation

For the forward model we have to define a true magnetic background field $\mathbf{B}_0$ and we can calculate the magnetic induction field $\mathbf{B}_{\mu_i}$ for each dipole μ_1, μ_2, μ_3 with the dipole expression derived in chapter 2.

As stated in section 4.1, earth's magnetic background field varies between 25 and 65 μT. In this experiment we define the magnetic background field as 50 μT in the y-direction:

$$\mathbf{B}_0 = \begin{bmatrix} 0 \\ 50 \\ 0 \end{bmatrix} \cdot 10^{-6} \tag{8.1}$$

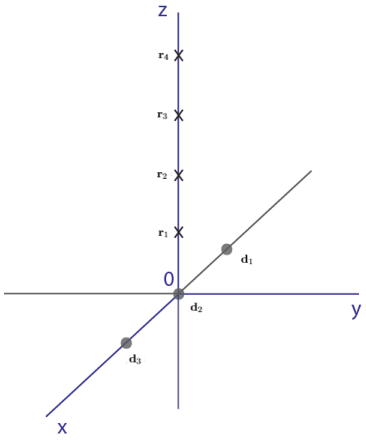

Figure 8.1: The situation on which the twin experiment is done.

We calculate each $\mathbf{B}_{\mu_i}$ forward, with $i = 1, 2, 3$ using MATLAB. We use these vectors to calculate the supposed measured, total magnetic field $\mathbf{B}$ on locations $\mathbf{r}_j$ with $j = 1, 2, 3, 4$. Solving the forward problem, means we have to calculate this $\mathbf{B}(\mathbf{r}_j)$. We use the following:

$$\mathbf{B}(\mathbf{r}_j) = \mathbf{B}_0 + \sum_{i=1}^{3} \mathbf{B}_i \tag{8.2}$$

8.2 Inverse simulation

Now, for solving the inverse problem, suppose the vector of measurements $\mathbf{B}(\mathbf{r})$, given by (8.2), is known. The magnetic background field $\mathbf{B}_0$ and induction field of every dipole $\mathbf{B}_{\mu_i}$ is unknown. Using the three different methods, we try to find the original magnetic background field $\mathbf{B}_0$. We use the method of least squares (a direct solver), truncated singular value decomposition, and the method of conjugate gradient least squares. The field we obtained by solving the inverse problem via these three different methods is denoted by $\mathbf{B}_0^c$. To determine if the model computes an acceptable solution, we will compare $\mathbf{B}_0$ and $\mathbf{B}_0^c$ in this experiment using the approximation errors.

The direct solver does not need any choosing of parameters. However, we do need to choose a regularization parameter for the TSVD.

8.2.1 Regularization parameter for the TSVD

For the TSVD, the singular values σ_i for $i = 1, .., r$ of a matrix A that is to be in inverted, and $r = rank(A)$ are ordered from larger values to smaller values on the diagonal of a matrix Σ. The regularization parameter k with $k < r$ should be chosen such that only the first k singular values are taken into account. In this twin experiment with $M = 4$ measurements and $N = 3$ dipoles, we have a linear system with a (12×12)-matrix A. This means there are $r = 12$ singular values of A. If we compute Σ and look at the diagonal with ordered singular values, we find:

k = 1	k = 2	k = 3	k = 4	k = 5	k = 6
2.0	2.0	2.0	$1.7 \cdot 10^{-7}$	$1.0 \cdot 10^{-7}$	$9.0 \cdot 10^{-8}$

k=7	k = 8	k = 9	k = 10	k = 11	k = 12
$9.6 \cdot 10^{-9}$	$6.3 \cdot 10^{-9}$	$3.7 \cdot 10^{-9}$	$4.5 \cdot 10^{-10}$	$3.8 \cdot 10^{-10}$	$2.8 \cdot 10^{-18}$

We see that there is jump from larger values to smaller values at the fourth and eleventh singular value. We can choose either which produces a better solution. For this experiment we choose the regularization parameter $k = 11$.

8.2.2 Running the solvers

Using this regularization parameter $k = 11$ for the TSVD, we have found the following solution for $\mathbf{B}_0^c$:

$$\mathbf{B}_0^c = \begin{bmatrix} 0.11 \\ 49.9 \\ 0.12 \end{bmatrix} \cdot 10^{-6} \tag{8.3}$$

Each component of $\mathbf{B}_0^c$ represents the area density of the magnetic flux in the x, y and z-directions respectively. One could say the

Running the iterative solver, we find the following solution using the CGLS:

$$\mathbf{B}_0^c = \begin{bmatrix} -0.30 \\ 49.8 \\ -0.08 \end{bmatrix} \cdot 10^{-6} \tag{8.4}$$

Recall the true magnetic background field $\mathbf{B}_0$ to be:

$$\mathbf{B}_0 = \begin{bmatrix} 0 \\ 50 \\ 0 \end{bmatrix} \cdot 10^{-6}$$

We can see both solutions obtained with the TSVD and CGLS are almost the exact same as the true magnetic background field $\mathbf{B}_0$ we defined in the forward problem. However the direct solver does not work so well. Now that we have calculated $\mathbf{B}_{0c}$ with three different solvers, we will do a proper comparison between the three solutions.

8.3 Comparison between the solutions

As explained in section 5.5 we can use the approximation errors to determine whether the solutions obtained above are acceptable, telling us whether the system is consistent. We have calculated both the absolute and relative error for all three solvers. The results are shown below.

Method	Absolute error	Relative error
Direct solver	NaN	NaN
TSVD	$2.18 \cdot 10^{-6}$	$4.35 \cdot 10^{-2}$
CGLS	$9.87 \cdot 10^{-7}$	$1.97 \cdot 10^{-2}$

We see that the direct solver computes 'NaN', meaning the solver can not compute a number. This means the method is not working well at all. This disastrous result was to be expected because the condition number of the problem is very high, namely $\kappa(A) \sim 10^{17}$, which is why we need regularization. Also, as explained in section 6.4, the method relies on dividing by the singular values of A and as we can see in the table above, these values are incredibly small, causing the solution obtained by the method of least squared to blow up, this causes the 'NaN'-result.

The TSVD and CGLS both have a error percentes of less then 10%, making both solutions an acceptable approximation of $\mathbf{B}_0$. Also, the difference between the solutions obtained by the TSVD and CGLS abd the true $\mathbf{B}_0$ is nearly zero. The TSVD has a smaller absolute and relative error than the CGLS, meaning that for this particular experiment, the TSVD is a better method.

8.4 Further experimenting

In order to make sure the conducted twin experiment is not a special, lucky case, where the prediction model, using the TSVD or CGLS, performs well, we can experiment further with the placement of the dipoles or magnetic moments. The actual research consisted of experimenting with the amount of measurements M and amount of dipoles N. The results of several cases can be found in the appendix. For every experiment we find that the prediction model computes an accurate approximation of the magnetic background field.

8.5 Concluding the twin experiment

We have found three different solutions to a linear system $A\mathbf{x} = \mathbf{b}$, where A is the matrix depending on the amount of measurements $M = 4$ and amount of dipoles $N = 3$, and $\mathbf{b}$ is the vector containing the measurements on locations $\mathbf{r}_j$ with $j = 1, 2, 3, 4$.

We used three different solvers, a direct solver: the method of least squares, a regularization method: the truncated singular value decomposition and the conjugate gradient least squares. After comparing the three solutions, using the approximation errors, we have come to the conclusion that the direct solver does not work well, as predicted. But using the TSVD or CGLS, we have a consistent model as we're able to calculate a magnetic background field $\mathbf{B}_0$ within the margins of error. Knowing that our model computes a good solution, we can start testing the model on real data obtained by the Seven Senors-array.

Chapter 9

The Seven Sensors Experiment

In this chapter we explain how the Seven Sensors experiment was conducted. The results can be found at the end of this chapter. The Seven Sensors is a sensor array that consists of seven magnetic sensors arranged as an array along a line. We can use this sensor array to create data of certain situations we wish to retrieve data of (i.e. measurements along a ships mast). We created two different situations:

- A setup that mimics the method the navy uses today. This method considers only one data point obtained from a single sensor in the top of the mast of a naval vessel, where a disturber (i.e. a ship) is present. We can use the Seven Sensors to recreate this situation by considering the top sensor, the seventh one, to be the sensor in the top of the mast and to put a steel plate below the sensors as the disturber. We simply ignore the data the other six sensors pick up.

- A setup that creates an environment for the new method. The new method uses the measurements of complete sensor array. Therefore, instead of only considering the top sensor, we consider all seven sensors.

We run the model on the data set from both situations and we see if there is any added value to the new method.

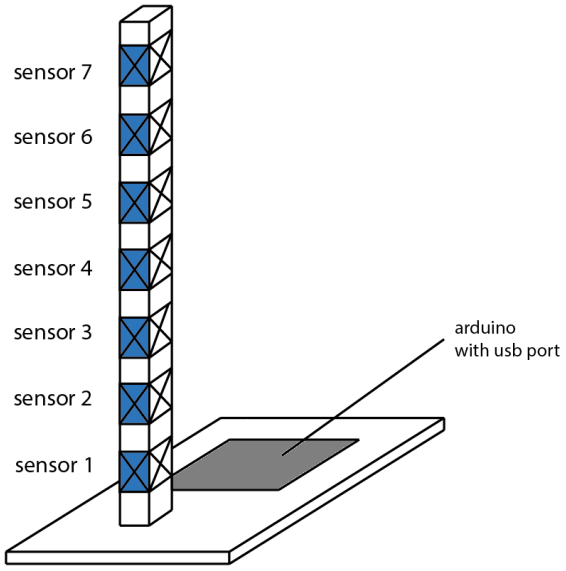

Figure 9.1: A schematic drawing of the Seven Sensors-array.

9.1 The setup

As mentioned before, the Seven Sensors is an sensor array consisting of seven sensors. It is attached to a little wooden plate (note that wood is non-magnetic material) with an arduino on it, see Figure 9.1. An arduino, see Figure 9.2, is a piece of computer hardware, a small computer, for building digital devices and interactive objects that can sense and control objects in the physical world. The sensors measure the magnetic field and the arduino converses this to a set of data points. We can connect the arduino to a laptop or computer, using a USB-cable, to take a look at the data and to use it for the model.

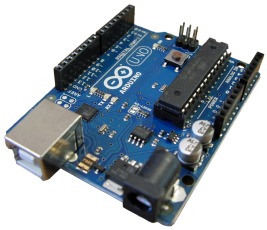

Figure 9.2: An arduino, attached to the wooden plate.

It is important that we implement the exact same measurements of the setup into our model. In the twin experiment, we chose the sensor locations with an distance of one meter from each other. However, this setup has a height of 35.7 centimeters and is obviously a much smaller setup than the simulated setup of the twin experiment. Therefore, we have to change the input for the sensor locations and the dipole locations according to the measurements of the setup, see Figure 9.3a.

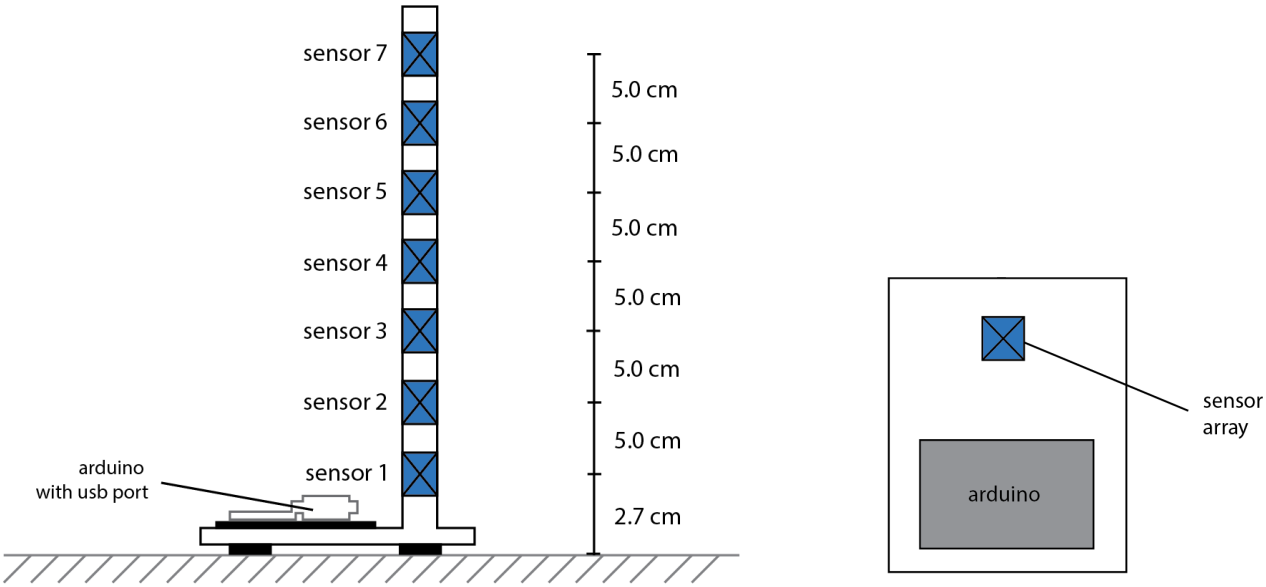

(a) A side view of the setup.

(b) A top view of the setup.

Figure 9.3: The measurements of the setup.

The setup shown in Figures 9.1, 9.3a and 9.3b is used to measure the true magnetic background field where no disturbance or dipoles are placed in its vicinity. When we want to measure the magnetic field when a disturber is in the vicinity of the sensors, mimicking a ship being near to sensor(s) in the mast, we put one or several steel plates below the Seven Sensors to create a disturbance. See the Figures 9.4 and 9.5.

We have four different plates of various thickness, all 30 by 30 centimeters. The idea behind this is that we increase the strength of the magnetic field. The more plates we consider, the more steel we have and thus a stronger field strength for the sensors to measure. We consider the place where the array is attached to be the origin and the array to be the z-axis. Appendix shows pictures of the setup.

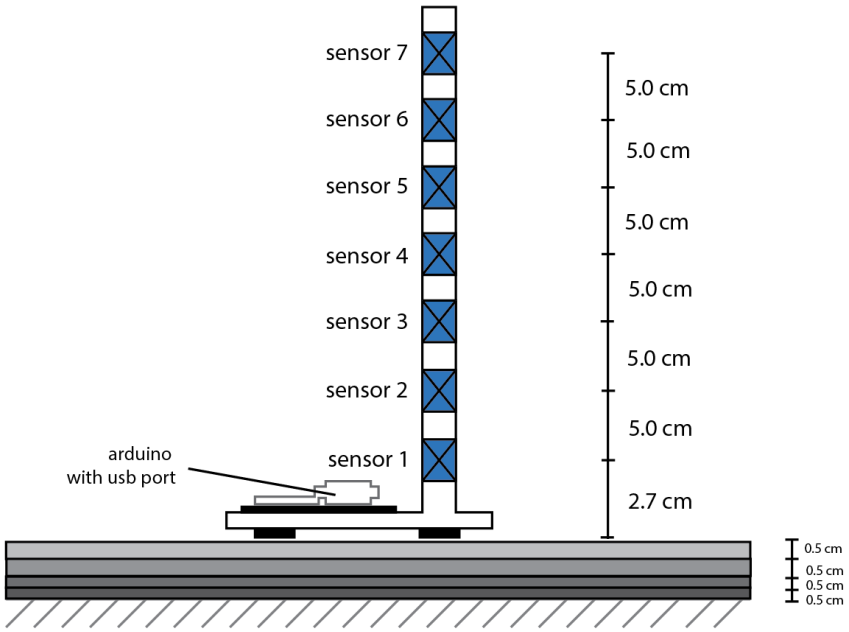

Figure 9.4: A side view of the setup with steel plates below the Seven Sensors.

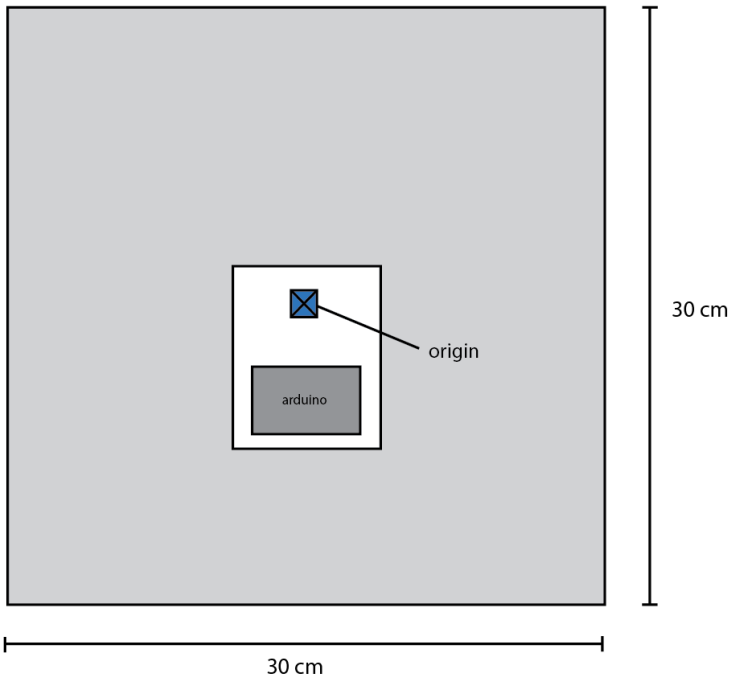

Figure 9.5: A top view of the setup with steel plates below the Seven Sensors.

9.2 The Method

Every sensor does one measurement of the magnetic field in the x, y and z-direction. This means one sensor on location $\mathbf{r}_j$ provides a vector $\mathbf{B}(\mathbf{r}_j) \in \mathbb{R}^3$, where $j \in \{1, 2, ..., 7\}$. This would mean that with seven sensors, we get seven vectors $\mathbf{B}(\mathbf{r}_1), \mathbf{B}(\mathbf{r}_2), ..., \mathbf{B}(\mathbf{r}_7)$. For one experiment, we consider only one $j \in \{1, 2, ..., 7\}$ to reproduce the current method that uses only a single sensor, whereas for the other experiment, we consider all $j = 1, 2, ..., 7$. To keep track of all the different notions and to distinguish between all the fields in this experiment, see Table 9.2.

$\mathbf{B}_0$	The true magnetic background field	[T]
$\mathbf{B}_0^m$	The measured magnetic background field. This notion is explained in section 9.2.1 Note that this field is obtained by the use of all sensors. A disturber is not present.	[T]
$\mathbf{B}(\mathbf{r}_j)$	The magnetic field measured by the sensor at location $\mathbf{r}_j$ Note that this field is obtained by the use of one sensor. A disturber may be present.	[T]
$\mathbf{B}_0^c$	The computed magnetic background field, obtained by the prediction model Note that this field is obtained by using all seven sensors. A disturber is present.	[T]
$\mathbf{B}_0^s$	This field is $\mathbf{B}(\mathbf{r}_j)$ at location $\mathbf{r}_j$, that is to be assumed the magnetic background field obtained by a single sensor Note that this field is obtained by the use of one sensor. A disturber is present.	[T]

Table 9.1: Symbols used to conduct the Seven Sensors experiment.

To see if the prediction model and use of the sensor array have any added value to the current method, we test both methods by comparing them to the original magnetic background field. Afterwards, we look at the approximation errors to determine which method predicts $\mathbf{B}_0$ more accurately. Before we do any comparisons between the existing method and the new method, we need some material to compare it to. In other words, we need to know what the true magnetic background field on the location of our setup is before we can run the model on both described situations. Therefore start by measuring the true magnetic background field.

9.2.1 Experiment 1: The true magnetic background field

The magnetic background field, denoted by $\mathbf{B}_0$, is the field we measure before running the prediction model. In other words, we observe no disturbers in this field. We compare the obtained $\mathbf{B}_0^s$ and $\mathbf{B}_0^c$ to this magnetic background field $\mathbf{B}_0$ to see if the prediction model computes accurate solutions for $\mathbf{B}_0$. We obtain the true magnetic background field $\mathbf{B}_0$ by measuring the field $\mathbf{B}_0^m$ in each sensor without a disturber (i.e., one or all of the steel plates). As the measurements are contaminated by noise, the magnetic background field in each sensor will differ slightly from the other. This is not what is supposed to happen as the earth's magnetic background field should be the same at every sensor location. To solve this problem, we consider a an average of all the measured values of the magnetic background field:

$$\mathbf{B}_0 := \mathbf{B}_0^m = \frac{1}{7} \sum_{i=1}^{7} \mathbf{B}^i \tag{9.1}$$

where $\mathbf{B}_i$ is the magnetic field at location $\mathbf{r}_i$ when no disturber is present. This constructed $\mathbf{B}_0$ is considered to be the true magnetic background field. The flow chart in Figure 9.6 describes what happens in experiment 1.

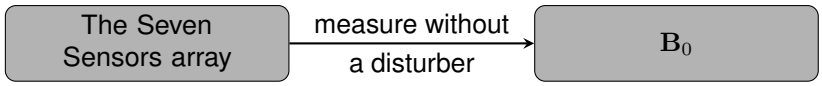

Figure 9.6: Measuring the true, uniform, magnetic background field.

9.2.2 Experiment 2: The method used today

To reproduce the the method we have today, which uses a single sensor on board a steel ship, we only consider the seventh sensor of the sensor array with a disturber present. We assume that the seventh sensor measures $\mathbf{B}_0$. The measured, magnetic field at location $j \in \{1, 2, ..., 7\}$ is denoted by $\mathbf{B}(\mathbf{r}_j)$. The magnetic background field this single sensor acquires is assumed to be this $\mathbf{B}(\mathbf{r}_j)$ and is denoted by $\mathbf{B}_0^s$. In this experiment, we used $j = 7$, as we imagined the top of the array to be the top of the mast where the sensor is placed in reality. Comparing $\mathbf{B}_0^s = \mathbf{B}(\mathbf{r}_j)$ to $\mathbf{B}_0$ shows us that this method works sufficiently well as the error's rule of thumb is satisfied. The results can be found in chapter 10.

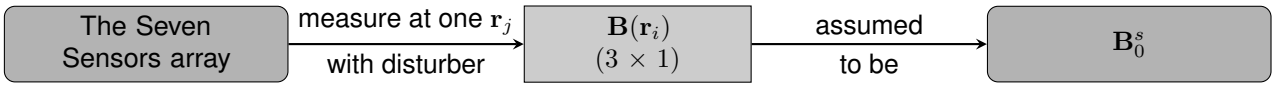

Figure 9.7: Assuming the measured field to be the amgnetic background field.

9.2.3 Experiment 3: The new method

The new method uses the whole sensor array. Therefore, instead of only considering one data point, we consider the complete data set the Seven Sensors provides. This means we measure all $\mathbf{B}(\mathbf{r}_j)$, where $j = 1, 2, ..., 7$. This results in a data set consisting seven data points, that is 21 different values because of the seven sensors times three components. We run the prediction model on this data set and find a new approximation for the magnetic background field, denoted by $\mathbf{B}_0^c$. This method also works sufficiently well.

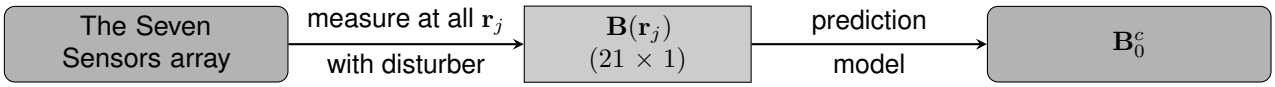

Figure 9.8: The model consisting of so

Now that we have conducted the complete Seven Sensors experiment on all situations, we can compare the results. The goal of this project, as stated in chapter one, is to find an accurate approximation $\mathbf{B}^c$ of $\mathbf{B}_0$ with the sensor array and prediction model and see if $\mathbf{B}^c$ is a better approximation of $\mathbf{B}_0$ than $\mathbf{B}^s$ is. The results are found at the end of this chapter.

9.2.4 Additional measurements 1

In experiment 2, we used the seventh sensor of the sensor array. However, looking at the dimensions of a naval ship, we see that the first or second sensor would make more sense as the sensor in the top of the mast, see Figure 9.9. For this reason, some additional measurements were done to see if $\mathbf{B}_0^c$ could be more accurate than $\mathbf{B}_0^s$ measured at all locations. Thus when analyzing the results we consider $\mathbf{B}^s = \mathbf{B}^i$, for *every* $i \in \{1, 2, ..., 7\}$.

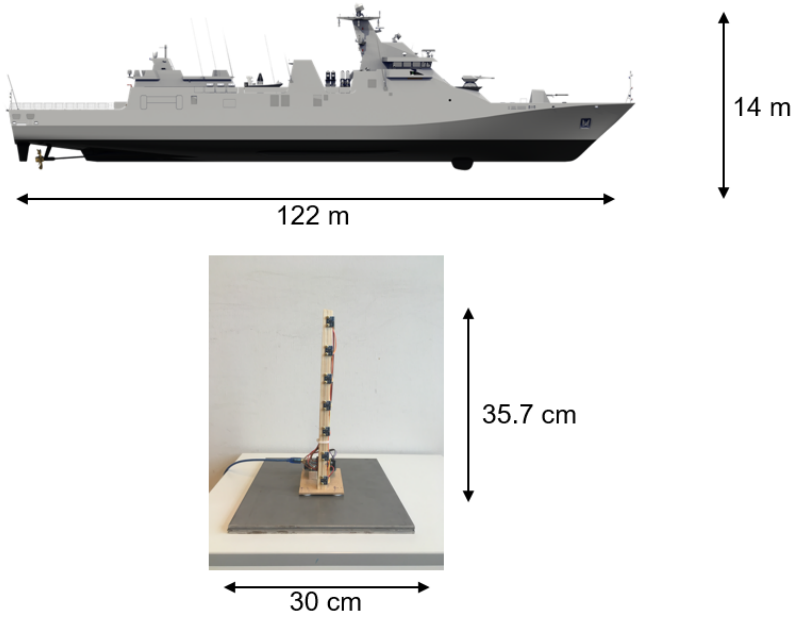

Figure 9.9: The difference between the dimensions of a naval ship and the Seven Sensors array

9.2.5 Additional measurements 2

Following up on section 9.2.4, we measure $\mathbf{B}(\mathbf{r}_j)$ at all seven locations $\mathbf{r}_1, \mathbf{r}_2, ..., \mathbf{r}_7$ and in chapter 10 we compare $\mathbf{B}_0^c$ to each field at every different location, to see if $\mathbf{B}_0^c$ is more accurate than $\mathbf{B}_0^s$ for every sensor. However, this means that, if we were to consider the second sensor to be the sensor in the top of the mast for the current situation, than in terms of the dimensions of the Seven Sensors-setup which has all its sensors 5 centimeters removed from each other, we do not have room for five more sensors above that second sensor. This means, for the new method, we can only consider the second sensor and everything below it, in other words, we have a sensor array of two sensors.

This second additional measurement compares the solutions $\mathbf{B}_0^s$, where $\mathbf{B}_0^s$ is measured at $\mathbf{r}_2$, and $\mathbf{B}_0^c$, where the sensor array only consists of two sensors.

Chapter 10

Results and prediction model analysis

This chapter reveals what we have found after conducting the measurement experiment and analyzes it after which a conclusion can be drawn.

10.1 Results

10.1.1 Experiment 1

In experiment 1, we measured the magnetic background field in each sensor. Because each measurement is slightly different from the other, which is not possible for the locally uniform background field, we assumed the mean of all measurements to be the magnetic background field. A plot of the x, y and z-components of the magnetic backgroundfied $\mathbf{B}_0$ can be found in Figure 10.1.

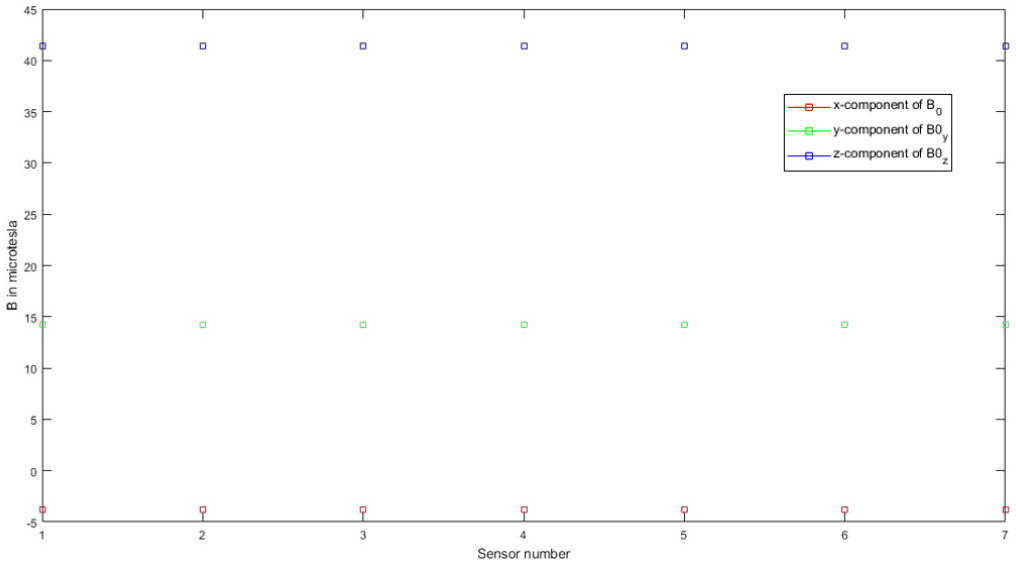

Figure 10.1: The measured magnetic background field in all seven sensors.

10.1.2 Experiment 2

For experiment 2, we measured the magnetic field in each sensor at location $\mathbf{r}_j$, with $j = 1, 2, ..., 7$. The current method assumes one of these measured fields $\mathbf{B}(\mathbf{r}_j)$ to be the magnetic background field. Hence, the current method assumes the following:

$$\mathbf{B}_0 = \mathbf{B}_0^s = \mathbf{B}(\mathbf{r}_j)$$

Figure 10.2 shows the true magnetic background field $\mathbf{B}_0$ compared to the field measured in each sensor, with a disturber present. We can see that the approximation

$$\mathbf{B}_0 = \mathbf{B}_0^s = \mathbf{B}(\mathbf{r}_7)$$

is very close to the true background field. This is possibly because, the method works really well or the seventh sensor is too far away, meaning the total measured field does not contain any distortion any more.

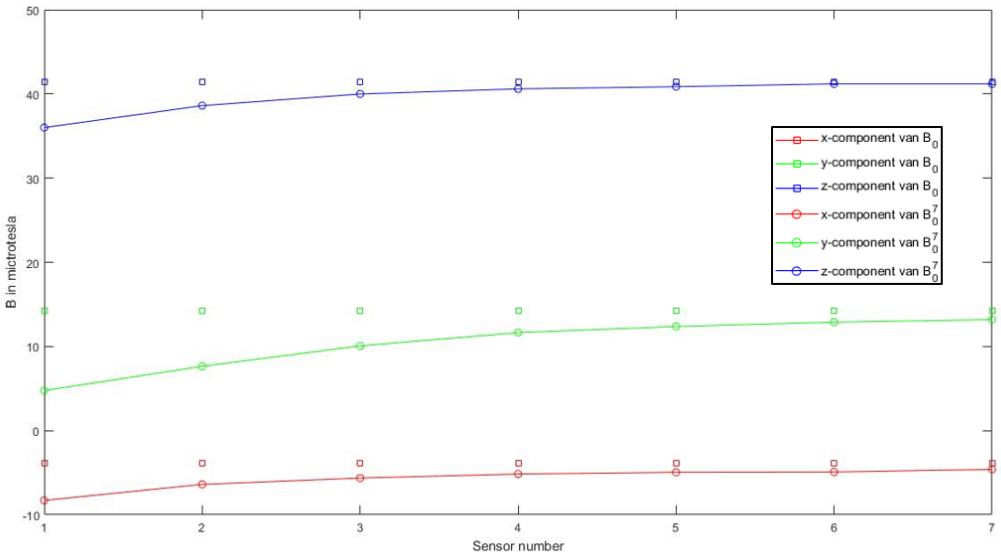

Figure 10.2: The magnetic field measured in each sensor, compared to the magnetic background field.

10.1.3 Experiment 3

One of the main goals was to determine if we could compute a more accurate magnetic background field using a dipole model and the sensor array. For experiment 3, we measured the magnetic field in each location $\mathbf{r}_j$ and we computed an approximation $\mathbf{B}_0^c$ of the magnetic background field $\mathbf{B}_0$ with a prediction model. Figure 10.3 shows a comparison between the true magnetic background field, the magnetic background fields obtained with a single sensor and the magnetic background field computed with a prediciton model and sensor array. Our approximation, the dotted lines are continuously closer to $\mathbf{B}_0$ than any $\mathbf{B}_0^s$ is.

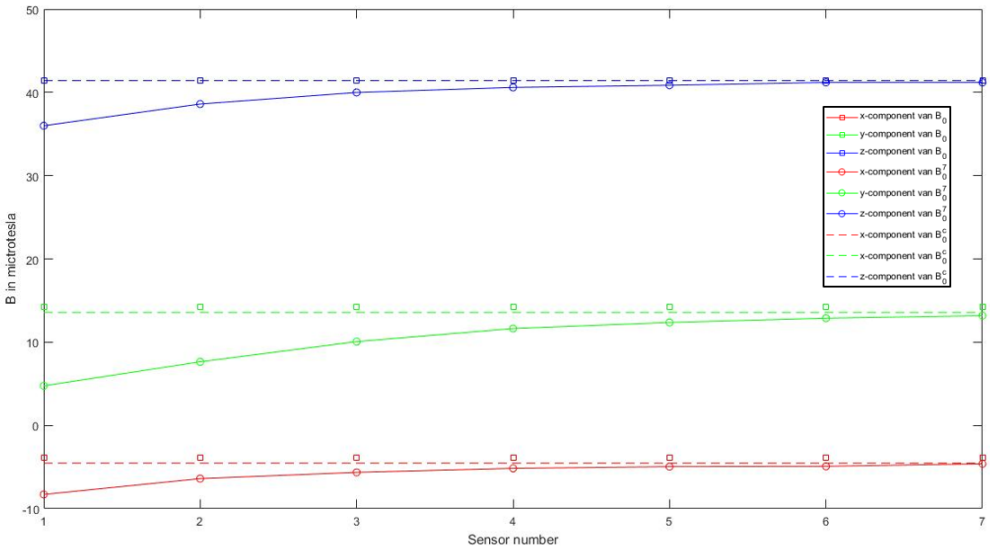

Figure 10.3: All experiments 1, 2 and 3.

10.2 Validation of the prediction model

The first goal of this research is to correctly formulate a prediction model that accurately determines the magnetic background field, using the sensor array. The prediction model, using the truncated singular value decomposition, computes an approximation for the magnetic background field $\mathbf{B}_0$. To determine if it is accurate, we need some reference material. Therefore, we measured the true $\mathbf{B}_0$ (experiment 1). See Figure 10.1. After running the prediction model we computed an approximation $\mathbf{B}_0^c$ of $\mathbf{B}_0$. Table 10.2 shows the components of $\mathbf{B}_0$ and $\mathbf{B}_0^c$ in microtesla. To determine if this result $\mathbf{B}_0^c$ for $\mathbf{B}$ is accurate, we calculated the approximation errors. See the table below.

component	B_0	B_0^c
x	-3.80	-4.53
y	14.2	13.57
z	41.4	41.4

Table 10.1: The true magnetic background field (left) and its the approximation (right) in microtesla.

Method	Absolute error	Relative error
Direct solver	1.32	$5.67 \cdot 10^{-1}$
TSVD	$9.67 \cdot 10^{-1}$	$2.20 \cdot 10^{-2}$
CGLS	$9.64 \cdot 10^{-1}$	$2.20 \cdot 10^{-2}$

Table 10.2: The approximation errors between of $\mathbf{B}_0^c$

We see that the approximation with the prediction model, using the TSVD, computes an acceptable solution. The absolute error is less then one, meaning every component in the approximation $\mathbf{B}_0^c$, differs no more than 0.97 μT from the components of the true magnetic background field. Also, the relative error shows us that the percent error of 2.20% is also within the acceptable error margin of 10%. We can conclude that we have determined an accurate description of the magnetic background field with $\mathbf{B}_0^c$. Therefore, the prediction model we formulated can be considered as valid.

10.3 Added value of the prediction model

We have seen that we can determine an accurate magnetic background field with the sensor array, and Figure 10.3 shows us that there is certainly some added value to the prediction model. The second goal of this research was to improve the method used today. Therefore, we conducted experiment 2 and compared the results to experiment 3.

component	B_0	B_0^c	$B(r_1)$	$B(r_2)$	$B(r_3)3$	$B(r_4)$	(r_5)	$B(r_6)$	$B(r_7)$
x	-3.84	-4.53	-8.29	-6.39	-5.64	-5.16	-4.96	-4.92	-4.61
y	14.2	13.6	4.76	7.64	10.1	11.6	12.4	12.9	13.2
z	41.4	41.4	36.0	38.6	40.0	40.1	40.1	41.2	41.2

Table 10.3: The magnetic background field for all different situations, using TSVD for the prediction model.

As previously stated, each $\mathbf{B}(\mathbf{r}_j)$, with $j \in \{1, 2, ..., 7\}$ represents the magnetic field at location $\mathbf{r}_j$. Each magnetic background field $\mathbf{B}_0^s$ obtained by the current method, so measured with a single sensor, is assumed to be the $\mathbf{B}(\mathbf{r}_j)$ for $j \in \{1, 2, ..., 7\}$. For example, to see if $\mathbf{B}_0^c$ is a more accurate approximation than the field measured with just the seventh sensor, we compute $\mathbf{B}_0^s = \mathbf{B}(\mathbf{r}_7)$. Finally, for every j we compare

$$\mathbf{B}_0^s = \mathbf{B}(\mathbf{r}_j)$$

and $\mathbf{B}_0^c$ independently to $\mathbf{B}_0$ to see if there is any added value to the prediction model. We have already determined that $\mathbf{B}_0^c$ is an accurate magnetic background field, however, to see if it is more accurate than $\mathbf{B}_0^s$ we calculated the approximation errors once more, see Table 10.3. We also see in Figure 10.1 and Figure 10.3.

Method	Absolute error	Relative error
Sensor 1	11.8	$2.68 \cdot 10^{-1}$
Sensor 2	7.60	$1.73 \cdot 10^{-1}$
Sensor 3	4.75	$1.08 \cdot 10^{-1}$
Sensor 4	3.02	$6.87 \cdot 10^{-2}$
Sensor 5	2.24	$5.10 \cdot 10^{-2}$
Sensor 6	1.74	$3.96 \cdot 10^{-2}$
Sensor 7	1.32	$3.01 \cdot 10^{-2}$
Direct solver	1.32	$5.67 \cdot 10^{-1}$
TSVD	$9.67 \cdot 10^{-1}$	$2.20 \cdot 10^{-2}$
CGLS	$9.64 \cdot 10^{-1}$	$2.20 \cdot 10^{-2}$

Table 10.4: The approximation errors between the sensor array and the seventh sensor.

We see that, for every sensor, both the absolute error and the relative error are smaller when using the sensor array and the TSVD or CGLS. This means the use of the sensor array computes a more accurate approximation of $\mathbf{B}_0$ than the current method does, using only one sensor. It does not matter which sensor would be the sensor in the top of the mast, as $\mathbf{B}_0^c$ is more accurate for $\mathbf{B}_0$ than the fields measured in all sensors. Also, we see that the CGLS is able to compute a smaller absolute error, but as the difference is really small, we could take either the TSVD or the CGLS as the relative errors are the same.

10.4 The result of additional measurements

The previous section already shows us that, if we have an array of seven sensors, it computes a more accurate magnetic background field than if we were to consider only a single sensor. However, to take into consideration more realistic dimensions of the problem, we also looked at a sensor array of two sensors and $\mathbf{B}_0^s = \mathbf{B}^2$. We found the following:

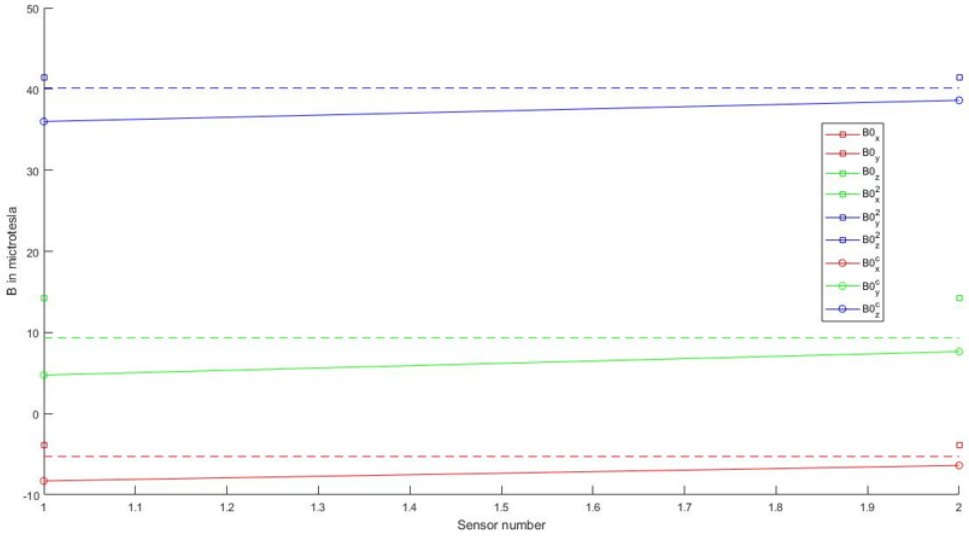

Figure 10.4: All experiments 1,2 and 3 when using a sensor array of two sensors

With the following components and approximation errors:

component	B_0	B_0^c	$B(r_2)$
x	-3.84	-5.28	-6.39
y	14.2	9.32	7.63
z	41.4	40.1	38.6

Table 10.5: The magnetic background field for all different situations, using TSVD for the prediction model.

Method	Absolute error	Relative error
Sensor 2	7.60	$1.73 \cdot 10^{-1}$
Direct solver	5.27	$1.20 \cdot 10^{-1}$
TSVD	5.27	$1.20 \cdot 10^{-2}$
CGLS	5.27	$1.20 \cdot 10^{-2}$

Table 10.6: The approximation errors between the sensor array and the seventh sensor.

When looking at Table 10.4, we see that the relative error is larger than the thumb rule of 10%. However, when we look at Figure 10.4, we see that the sensor array consisting of only two sensors, is still able to compute a more accurate magnetic background field $\mathbf{B}_0^c$ than a single sensor would. We see that for $M = 2$ measurements, and $N = 1$ dipole, the direct solver performs good too. It might be that the linear system $A\mathbf{x} = \mathbf{b}$ is directly solvable when A is only a (6×6)-matrix.

Chapter 11

Conclusion

The end of the Seven Sensors experiment concludes this research. This conclusion recalls the problem and research goals and summarizes the process to achieving the two main goals.

A naval mine is able to detect the change of the magnetic field around it from a certain distance. A possible cause for this change is a naval ship passing by. The steel of a naval ship induces a magnetic field, also called the magnetic signature of a naval ship, which disturbs the magnetic field the naval mine is observing and the change is detected. The magnetic sensor on a mine constantly measures the total magnetic field at some location which consists of the earth's magnetic background field and any other magnetic field induced by steel objects at that same location.

The ultimate goal, that is a goal beyond this research, is to reduce the magnetic visibility of a naval ship such that a naval mine will not detect any change in the magnetic field. In other words, if it is possible to reduce the magnetic signature with a degaussing system to such an extent that the naval mine no longer measures change, there is a greater chance at avoiding risk of detonation.

In order to reduce the magnetic signature we have to know the magnetic background field, therefore this project focused on determination of the magnetic background field. The two main goals of this research, as defined in the introduction, are as followed:

- **Determination of the magnetic background field**. The first main goal is to determine an accurate approximation of the magnetic background field using a sensor array for measurements.
- **Improve the current method**. The second main goal is to improve the method that is used today, obtaining data by a single sensor.

The prediction model, based on inverse modeling, separates the magnetic background field from other existing, observed magnetic fields (i.e., the field induced by a ship). We tested the model on a simulation and afterwards on a smaller setup to investigate the possibilities for a larger naval ship. The goals of this research are achieved by investigating four essential topics. The topics as defined in chapter one are:

- **Determination of a correct formulation of the prediction model**.
- **Accuracy of the prediction model using the sensor array**.
- **Recreation of the existing method using one sensor**.
- **The value of the prediction model using the sensor array**.

The next section walks through every topic to explain how we can conclude the main goals are achieved.

11.1 Determination of a correct formulation of the prediction model using the sensor array

The prediction model is introduced in chapter six and revised after discussing the regularization methods in chapter eight, resulting in a correct formulation of the model that we tested and used. The prediction model consists of solving an inverse problem.

We know that the total magnetic field $\mathbf{B}$ measured at some location $\mathbf{r}$ is given by the sum of the magnetic background field $\mathbf{B}_0$ and the magnetic field induced by the steel object Ω.

$$\mathbf{B} = \mathbf{B}_0 + \mathbf{B}_\Omega$$

We replaced the steel object Ω by several magnetic point dipoles and the dipole model computes the solution $\mathbf{B}_0^c$, which is an approximation of the magnetic background field $\mathbf{B}_0$.

Therefore the prediction model solves the following inverse problem as stated in chapter 5:

The inverse problem. *Given the measured induction field $\mathbf{B}(\mathbf{r}_j)$, known sensor positions $\mathbf{r}_j$ with $j = 1, 2, ..., M$ and known dipole positions $\mathbf{d}_i$, where $i = 1, 2, ..., N$. Find the magnetic background field $\mathbf{B}_0$ and magnetic moments $\mathbf{m}_i$, for $i = 1, 2, ..., N$.* We solved the inverse problem, by rewriting the problem as a linear system

$$A\mathbf{x} = \mathbf{b}$$

The new method that uses a sensor array and a dipole model, performs truncated singular value decomposition to solve the linear system:

When translating this to the physics of a naval ship at sea, the matrix A is dependent on the sensor locations, the ship's location and the magnetic moment of the ship. The vector $\mathbf{b}$ represents the measurements obtained by the sensors in the array.

We have seen in chapter nine, that the prediction model performs a good approximation of a simulated magnetic background field. Because we were able to establish that the formulation of the model was correct, we were good to go on testing the model on real data. In addition to the twin experiment, we have found that the prediction performed works well on the experiment using real data too. For explanation of the validation of the model, see the next topic. The validation of the prediction model tells us that the computed solution is a good approximation of the original background field. Therefore, we can conclude that a correct formulation for the prediction model, that uses the sensor array, is achieved.

11.2 Accuracy of the prediction model using the sensor array

The previous topic confirms that the formulation of the prediction model is correct. Determining whether the prediction model computes an accurate approximation, is first discussed in chapter nine, where the twin experiment takes place. We use the approximation errors and a rule of thumb to see if the correct formulation of the prediction model also computes an accurate approximation of the magnetic background field.

The approximation errors are given by:

Approximation errors. Let a value v' be the approximation of v, then the absolute error is given by

$$\epsilon = \|v - v'\|$$

And the relative error is given by

$$\tau = \frac{\|v - v'\|}{v}$$

We see that the approximation errors are almost zero, meaning our solution for the simulated background field is more or less the exact same as the original simulated background field. However, in order for the prediction model to work, we had to perform regularization.

We used the truncated singular value decomposition to make the problem less sensitive to noise. We found that after regularization, the condition number of the matrix A of the linear system was lower than before regularization. A high condition number of A means we might have an ill-conditioned problem and therefore we should be more careful when interpreting the solution.

Having established that the prediction model seems to work, we tested it on the Seven Sensors data and we came to find that, with the use of the TSVD, the prediction model works well again. The computed magnetic background field has a maximum error of 0.97 μT. This means that the components of the computed magnetic background field differs no more than 1 μT from the original background field. Intuitively, this can be considered as good, but in addition, the relative error also tells us that the prediction model computes an accurate solution. We have a relative error of 2.20%. This satisfies the rule of thumb that says, the solution is not allowed to deviate more than 10% from the original solution.

A visualization of the solution also confirms that the approximation of the magnetic background field is accurate. The image below tells us that the computed solution obtained by the Seven Sensors is indeed very close to the original solution.

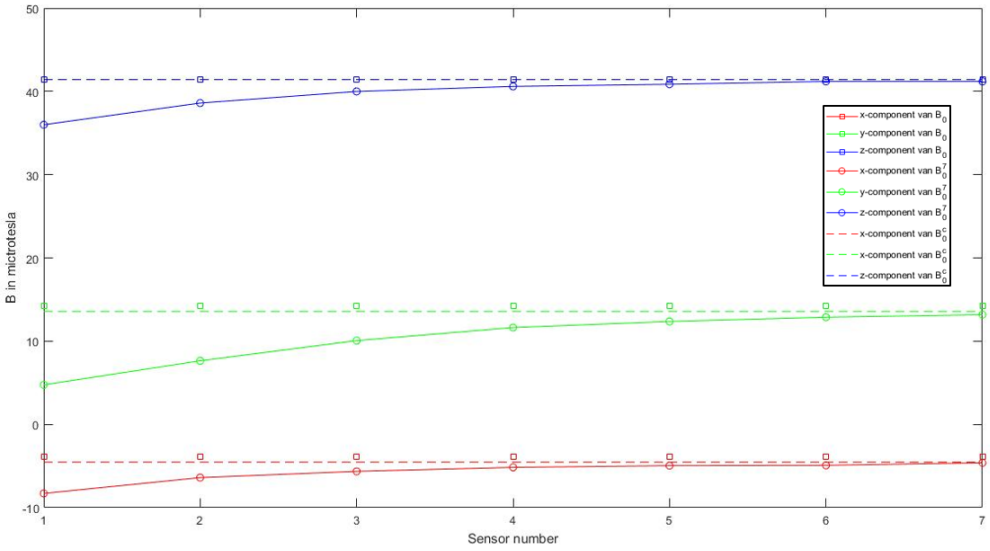

Figure 11.1: All experiments 1, 2 and 3.

11.3 Recreating of the existing method using one sensor

Besides formulating a prediction model to determine the magnetic background field accurately, the other goal of this research was to see if the new method with prediction model and sensor array has any added value to the current method. The current method does not use any dipole and only uses one sensor. In order to explore possible improvements of the current method, we recreated it for the purpose of referencing. We used the Seven Sensors to create data as the current would do. Thus instead of taking on all the data the Seven Sensors provided, we considered only one sensor and compared it to our computed solution. We did this for all sensors and analyzed the results, to see if we came up with an improved method. For a summary of the results see the next topic.

Considering only the seventh sensor can be seen as the worst case for our model. Because of the low magnetizing ability of the steel, a seventh sensor would be almost too far away, and the steel would not be detected anymore. Meaning the field measured in the seventh sensor is always going to be very close the original magnetic background field. However, more realistically, one should consider the first or second sensor when conducting this experiment. Comparing the dimensions of a naval vessels (e.g., a frigate), which has dimensions 122×14 meters, to the dimensions of 0.3×0.3 meters of our plate, the first or second sensor would agree with a realistic sensor and mast.

11.4 The value of the prediction model using the sensor array

We researched the value of the prediction that uses the sensor array. We compared our solution $\mathbf{B}_0^c$ to every magnetic background field $\mathbf{B}_0^s$ that was obtained by measuring the magnetic field $\mathbf{B}_0(\mathbf{r}_j)$ at each sensor location

$$\mathbf{r}_j$$

with $i = 1, 2, ..7$. We came to find that even for the worst case for our model, the seventh sensor, the prediction model still approximated the original background solution more accurately than the current method. Both visualization and approximation errors show us that, for every sensor, the prediction model works better than the current approach, see Figure 10.3.

Taking into consideration the dimensions of a frigate, we also compared the approximations of $\mathbf{B}_0$ obtained by taking the second sensor as the single sensor and obtained by using a sensor array consisting of two sensors. The approximation errors tell us that the computed magnetic background field $\mathbf{B}_0^c$ via the sensor array and prediction model is not accurate enough. However, we can see that is still more accurate than the current method that uses a single sensor.

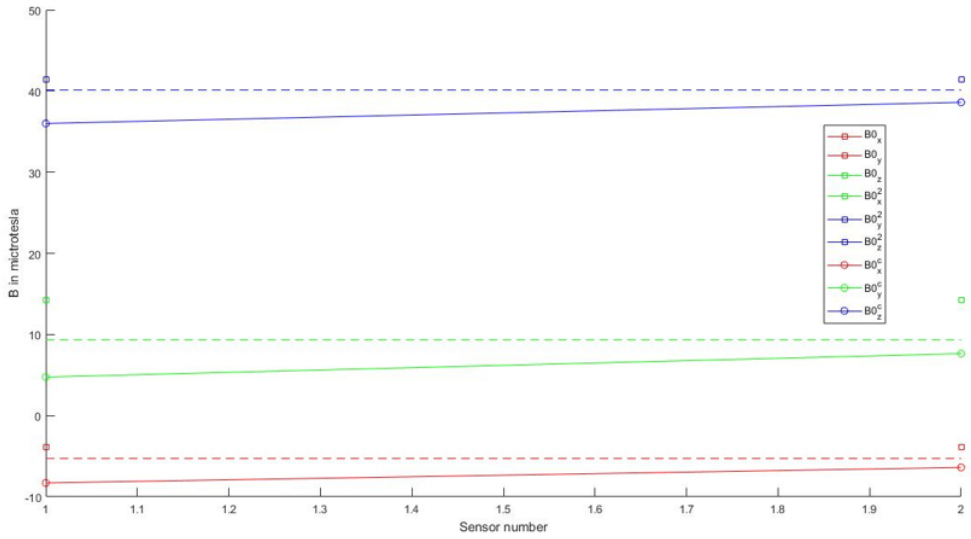

Figure 11.2: All experiments 1,2 and 3 when using a sensor array of two sensors

11.5 Further research

Even though the goals for this project, for seven sensors, were achieved, there is so much more to further investigate. This section explains only a few short ideas that could be considered as further research.

11.5.1 Dimensions of the setup

During this project, a prediction model was developed and tested on a small setup. Obviously, it is a stepping stone, but the dimensions do not come close to a real naval ship. The idea of the Seven Sensors was to consider the seventh sensor as the sensor a mast of a naval ship would have on its mast. However, the dimensions of the Seven Sensors are not in proportion to the dimensions of the steel and mast of a real naval ship. When considering the dimensions of a naval ship, we should not compare our computed solution to the solution obtained by the seventh sensor, but the first or second sensor is more likely. Further research where the setup is expanded to greater dimensions, will possibly me more trustworthy as the prediction model would be tested on a more realistic setup..

11.5.2 The magnetic moment of the dipole

The prediction model that inversely solves the linear system

$$A\mathbf{x} = \mathbf{b}$$

actually computes a solution that contains, not only the components of the magnetic background field, but also the magnetic moment of the dipole. Recall that the solution obtained with the truncated singular vlaue decomposition is given by:

$$\hat{\mathbf{x}} = \begin{bmatrix} B_{0x} \\ B_{0y} \\ B_{0z} \\ m_x \\ m_y \\ m_z \end{bmatrix}$$

We have complete neglected these values for $\mathbf{m} = [m_x \quad m_y \quad m_z]$ in this project. This is also where a lot of difficulties lie, hence, further research, one could take these values into consideration and try to approximate the magnetic moment of a steel object accurately.

It also would not matter if we considered either the seventh, the second or any other sensor as the single sensor. Table 10.3 tells us that a sensor array of seven sensors will always compute a more accurate magnetic background field

Appendix A

Derivation of equation (2.22)

Note that the dirac delta function has the following properties:

$$\int_{x=-\infty}^{\infty} f(x)\delta(x)dx = f(0) \tag{A.1}$$

$$\int_{x=-\infty}^{\infty} \delta(x-a)\phi(x) = \phi(a) \tag{A.2}$$

In chapter 2, we had derived the following for the potential $\varphi(\mathbf{r})$

$$\varphi(\mathbf{r}) = \frac{1}{4\pi} M_0 \pi a^2 \int_{x'=-\infty}^{\infty}\int_{y'=-\infty}^{\infty}\int_{z'=-\infty}^{\infty} \frac{[\delta(x'+l)-\delta(x'-l)]\cdot\delta(y')\cdot\delta(z')}{\sqrt{(x-x')^2+(y-y')^2+(z-z')^2}}\cdot dx'dy'dz'$$

Integrating with respect to z', makes $[\delta(x'+l)-\delta(x'-l)]\cdot\delta(y')$ a constant, and so

$$\varphi(\mathbf{r}) = \frac{1}{4\pi} M_0 \pi a^2 \int_{x'=-\infty}^{\infty}\int_{y'=-\infty}^{\infty} [\delta(x'+l)-\delta(x'-l)]\cdot\delta(y') \cdot \int_{z'=-\infty}^{\infty} \frac{1}{\sqrt{(x-x')^2+(y-y')^2+(z-z')^2}}\cdot\delta z'\cdot dz'dy'dx'$$

Now we use property (B.1) and suppose $f(z') = \frac{1}{\sqrt{(x-x')^2+(y-y')^2+(z-z')^2}}$.
We find

$$\begin{aligned}
\varphi(\mathbf{r}) &= \frac{1}{4\pi} M_0 \pi a^2 \int_{x'=-\infty}^{\infty}\int_{y'=-\infty}^{\infty} [\delta(x'+l)-\delta(x'-l)]\cdot\delta(y')\cdot f(0)\cdot dy'dx' \\
&= \frac{1}{4\pi} M_0 \pi a^2 \int_{x'=-\infty}^{\infty}\int_{y'=-\infty}^{\infty} [\delta(x'+l)-\delta(x'-l)]\cdot\delta(y')\cdot \frac{1}{\sqrt{(x-x')^2+(y-y')^2+(z-0)^2}}\cdot dy'dx' \\
&= \frac{1}{4\pi} M_0 \pi a^2 \int_{x'=-\infty}^{\infty}\int_{y'=-\infty}^{\infty} [\delta(x'+l)-\delta(x'-l)]\cdot\delta(y')\cdot \frac{1}{\sqrt{(x-x')^2+(y-y')^2+z^2}}\cdot dy'dx'
\end{aligned}$$

Now we integrate with respect to y' and this goes in the same manner, using property (B.1).

$$\begin{aligned}
\varphi(\mathbf{r}) &= \frac{1}{4\pi} M_0 \pi a^2 \int_{x'=-\infty}^{\infty}\int_{y'=-\infty}^{\infty} [\delta(x'+l)-\delta(x'-l)]\cdot\delta(y')\cdot \frac{1}{\sqrt{(x-x')^2+(y-y')^2+z^2}}\cdot dy'dx' \\
&= \frac{1}{4\pi} M_0 \pi a^2 \int_{x'=-\infty}^{\infty} [\delta(x'+l)-\delta(x'-l)]\cdot \int_{y'=-\infty}^{\infty} \frac{1}{\sqrt{(x-x')^2+(y-y')^2+z^2}}\cdot\delta(y')\cdot dy'dx' \\
&= \frac{1}{4\pi} M_0 \pi a^2 \int_{x'=-\infty}^{\infty} [\delta(x'+l)-\delta(x'-l)]\cdot f(0)\cdot dx' \\
&= \frac{1}{4\pi} M_0 \pi a^2 \int_{x'=-\infty}^{\infty} [\delta(x'+l)-\delta(x'-l)]\cdot \frac{1}{\sqrt{(x-x')^2+y^2+z^2}}\cdot dx'
\end{aligned}$$

Summarizing everything we have found, the potential is given by

$$\begin{aligned}
\varphi(\mathbf{r}) &= \frac{1}{4\pi} M_0 \pi a^2 \int_{x'=-\infty}^{\infty} [\delta(x'+l) - \delta(x'-l)] \cdot \frac{1}{\sqrt{(x-x')^2+y^2+z^2}} \cdot dx \\
&= \frac{1}{4\pi} M_0 \pi a^2 \left(\left[\int_{x'=-\infty}^{\infty} \delta(x'+l) \cdot \frac{1}{\sqrt{(x-x')^2+y^2+z^2}} \cdot dx \right] \right. \\
&\left. - \left[\int_{x'=-\infty}^{\infty} \delta(x'-l) \cdot \frac{1}{\sqrt{(x-x')^2+y^2+z^2}} \cdot dx \right] \right. \\
&= \frac{1}{4\pi} M_0 \pi a^2 \left(\frac{1}{\sqrt{(x+l)+y^2+z^2}} - \frac{1}{\sqrt{(x-l)+y^2+z^2}} \right) \qquad \text{by property (B.2)}
\end{aligned}$$

We used property (B.2). Note that that in the first term of the equation, we used that $\delta(x-a) = \delta(x'+l)$ and $a = -l$. In the second part of the equation, we used that $\delta(x-a) = \delta(x'-l)$ and $a = l$.

In conclusion, we've found equation (2.12)

$$\varphi(\mathbf{r}) = \frac{1}{4\pi} M_0 \pi a^2 \left[\frac{1}{\sqrt{(x+l)^2+y^2+z^2}} - \frac{1}{\sqrt{(x-l)^2+y^2+z^2}} \right]$$

Appendix B

Results of the twin experiment

Method	Absolute error	Relative error
Direct solver	NaN	NaN
TSVD	$2.07 \cdot 10^{-7}$	$4.15 \cdot 10^{-3}$
CGLS	$3.51 \cdot 10^{-7}$	$7.02 \cdot 10^{-3}$

$$\begin{aligned} \mathsf{d}_1 &= [-1 \quad 0 \quad 0]^T \\ \mathsf{d}_2 &= [0 \quad 0 \quad 0]^T \\ \mathsf{d}_3 &= [1 \quad 0 \quad 0]^T \end{aligned}$$

$$\begin{aligned} \mathsf{m}_1 &= [100 \quad 0 \quad 0]^T \\ \mathsf{m}_2 &= [100 \quad 0 \quad 0]^T \\ \mathsf{m}_3 &= [100 \quad 0 \quad 0]^T \end{aligned}$$

Method	Absolute error	Relative error
Direct solver	$1.32 \cdot 10^{-7}$	$1.32 \cdot 10^{-7}$
TSVD	$7.05 \cdot 10^{-7}$	$1.41 \cdot 10^{-2}$
CGLS	$8.96 \cdot 10^{-7}$	$1.79 \cdot 10^{-2}$

$$\begin{aligned} \mathsf{d}_1 &= [1 \quad 0 \quad 0]^T \\ \mathsf{d}_2 &= [0 \quad 0 \quad 0]^T \\ \mathsf{d}_3 &= [1 \quad 1 \quad 0]^T \end{aligned}$$

$$\begin{aligned} \mathsf{m}_1 &= [200 \quad 0 \quad 0]^T \\ \mathsf{m}_2 &= [0 \quad 0 \quad 0]^T \\ \mathsf{m}_3 &= [100 \quad 0 \quad 0]^T \end{aligned}$$

Method	Absolute error	Relative error
Direct solver	NaN	NaN
TSVD	$1.99 \cdot 10^{-6}$	$3.99 \cdot 10^{-2}$
CGLS	$8.38 \cdot 10^{-7}$	$1.68 \cdot 10^{-2}$

$$\begin{aligned} \mathsf{d}_1 &= [-1 \quad 0 \quad 0]^T \\ \mathsf{d}_2 &= [0 \quad 0 \quad 0]^T \\ \mathsf{d}_3 &= [1 \quad 0 \quad 0]^T \end{aligned}$$

$$\begin{aligned} \mathsf{m}_1 &= [50 \quad 10 \quad 0]^T \\ \mathsf{m}_2 &= [0 \quad 20 \quad 0]^T \\ \mathsf{m}_3 &= [0 \quad 0 \quad 100]^T \end{aligned}$$

Method	Absolute error	Relative error
Direct solver	NaN	NaN
TSVD	$2.0725 \cdot 10^{-7}$	$4.1450 \cdot 10^{-3}$
CGLS	$3.5107 \cdot 10^{-7}$	$7.0214 \cdot 10^{-3}$

$$\begin{aligned} \mathsf{d}_1 &= [1 \quad 0 \quad 0]^T \\ \mathsf{d}_2 &= [0 \quad 0 \quad 0]^T \\ \mathsf{d}_3 &= [2 \quad 0 \quad 0]^T \end{aligned}$$

$$\begin{aligned} \mathsf{m}_1 &= [0 \quad 100 \quad 0]^T \\ \mathsf{m}_2 &= [0 \quad 10 \quad 0]^T \\ \mathsf{m}_3 &= [0 \quad 0 \quad 100]^T \end{aligned}$$

Table B.1: The approximation errors of experiments with varying dipole location and magnetic moment.

Appendix C

Photos of the Seven Sensors setup

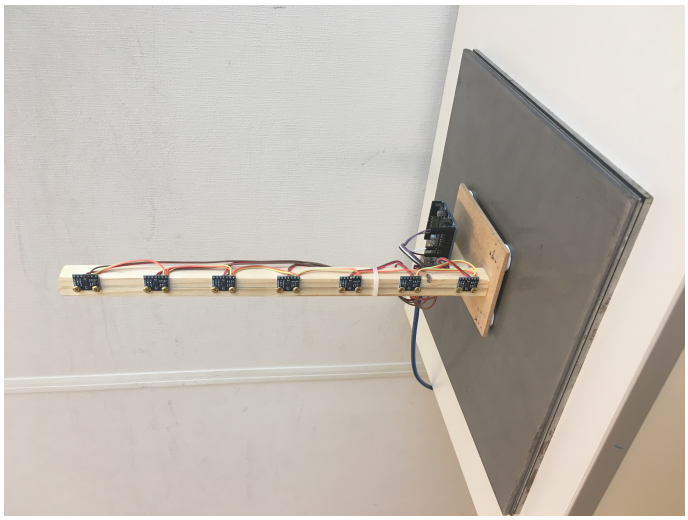

Figure C.1: The Seven Sensors array with a disturber

Figure C.2: A disturber (i.e., a steel plate or naval ship)

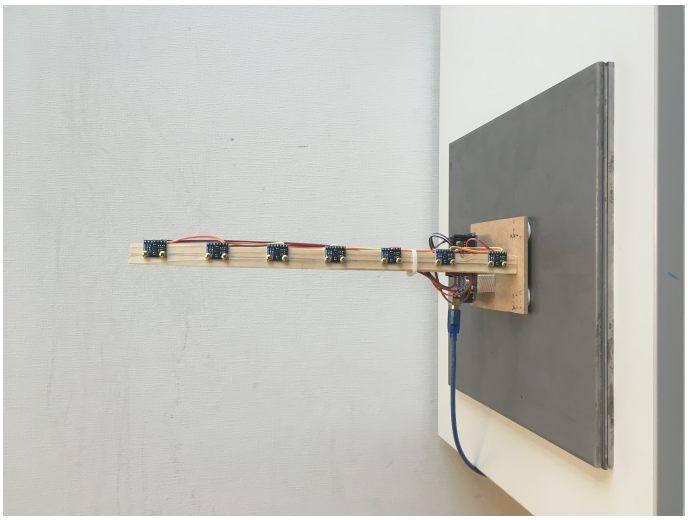

Figure C.3: The front view of the Seven Sensors

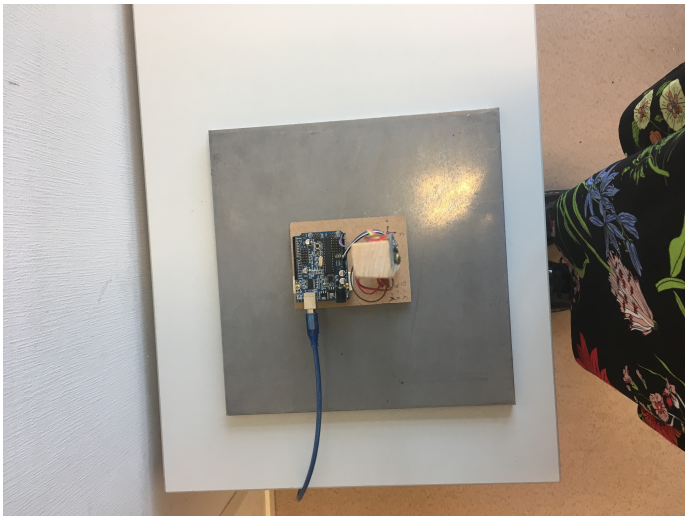

Figure C.4: The top view of the Seven Sensors

Bibliography

[1] A.R.J.P. Vijn *Inverse Modeling for Magnetic Signature Monitoring of Naval Ships*. MSc Thesis submitted to the Delft Institute of Applied Mathematics, Delft University of Technology, January 2016.

[2] Rwm Italia, S.p.A., A Rheinmetall Defence company *Manta. Antilanding shallow water mine*

[3] CSSM

[4] EMCoS Consulting and Software *Magnetic Signature of Naval Ship in the Earth's Magnetic Field* http://www.emcos.com/

[5] Walker, Barry, C. *Superposition of Magnetic Fields* University of Delaware, 2001

[6] John J. Holmes *Exploitation of A Ship's Magnetic Field Signatures*. Naval Surface Warfare Centre, West Bethesda, Maryland, USA, 2006.

[7] Naval Technology http://www.naval-technology.com

[8] C. C. Finlay S. Maus C. D. Beggan T. N. Bondar A. Chambodut T. A. Chernova A. Chulliat V. P. Golovkov B. Hamilton M. Hamoudi R. Holme G. Hulot W. Kuang B. Langlais V. Lesur F. J. Lowes H. Lühr S. Macmillan M. Mandea S. McLean C. Manoj M. Menvielle I. Michaelis N. Olsen J. Rauberg M. Rother T. J. Sabaka A. Tangborn L. Tøffner-Clausen E. Thébault A. W. P. Thomson I. Wardinski Z. Wei T. I. Zvereva *Geophysical Journal International* Geophys J Int (2010) 183 (3): 1216-1230. https://academic.oup.com/gji/article-lookup/doi/10.1111/j.1365-246X.2010.04804.x

[9] Prof. Dr. Philippe C. Cattin, MIAC, University of Basel *Image Restoration: Introduction to Signal and Image Processing* April 26th, 2016 https://miac.unibas.ch/SIP/06-Restoration.html(6)

[10] Björk, A.
Numerical Methods For lEast Squares Problems
1996